

ec

NISP Performance Analysis Report

Ref. EUCL- MPI-NPS-RP-00079
Version: Issue 3
Date: 17/01/2012
Page: 1/78

Title:	NISP Performance Analysis Report
Reference :	EUCL- MPI-NPS-RP-00079
Issue :	3.0
Date :	18/01/2012
Custodian :	Anne Ealet

Authors:	Function:	Date:	Signature:
K.Jahnke	NISP Photometry Scientist	18/01/12	
A. Ealet	NISP Spectroscopy Scientist	18/01/12	
B. Garilli	End to end spectro simulation	18/01/12	
Other Contributors			
G. Seidel	Photometry Simulator	17/01/12	
R. Holmes	Previous NISP Photometry Scientist	16/01/12	
P. Franzetti	End-to-end Spectro Simulation	15/01/12	
E. Rossetti	Spectroscopy simulation	15/01/12	
J Zoubian	Spectroscopy simulation	15/01/12	
F.Marmol	Spectroscopy simulation	15/01/12	
Approved:		Date:	Signature:
T. Maciaszek	NISP Instrument PM	17/01/12	
Authorized:		Date:	Signature:
Y.Mellier	EUCLID Consortium Lead	18/01/12	

ec

NISP Performance Analysis Report

Ref. EUCL- MPI-NPS-RP-00079
Version: Issue 3
Date: 17/01/2012
Page: 2/78

ec

NISP Performance Analysis Report

Ref. EUCL- MPI-NPS-RP-00079
Version: Issue 3
Date: 17/01/2012
Page: 3/78

Issue	Date	Page	Description Of Change	Comment
0.05	24/03/11		Table of Contents	
0.1	15/04/11		Begin adding detail	
0.2	11/05/11		Significant update to all sections	
0.3	17/05/11		Significant update to all sections	
0.4	18/05/11		Minor Updates	
1.0	20/05/11		Final version	
2.09	17/01/12		Major update for SPR	Major update of most evaluations
3.0	18/01/12		Final version	Minor correction

The presented document is Proprietary information of the Euclid Consortium.

This document shall be used and disclosed by the receiving Party and its related entities (e.g. contractors and subcontractors) only for the purposes of fulfilling the receiving Party's responsibilities under the Euclid Project and that the identified and marked technical data shall not be disclosed or retransferred to any other entity without prior written permission of the document preparer.

Table of Contents

1. Purpose and Scope	9
2. Documents	10
2.1. Applicable documents.....	10
2.2. Reference documents	10
2.2.1. Euclid Project Reference Document.....	10
2.2.1. ECSS Reference Documents.....	11
3. Acronyms.....	12
4. Requirement flow down and verification	14
4.1. Photometry Requirement Modifications.....	15
4.2. Spectroscopic Requirements and modifications for PERD.....	16
5. Instrument Configuration.....	17
5.1. Common Parameters	17
5.2. Photometry Specific Parameters.....	17
5.3. Spectroscopy Specific Parameters	19
6. Photometric Mode	20
6.1. Point Spread Function.....	20
6.2. Applicable Requirements.....	21
6.2.1. R-WL.2.1-12	21
6.2.2. R-WL.2.1-13	22
6.2.3. R-WL.2.1-17	23
6.2.4. R-WL.2.1-18	23
6.2.5. R-WL.2.1-19	23
6.2.6. R-WL.2.1-20	24
6.2.7. R-WL.2.1-21	24
6.2.8. R-WS.2.2-3.....	26
6.2.9. R-WS.2.2-6.....	32
6.2.10. R-WS.2.2-7	32
6.2.11. R-WS.2.2-10.....	34
6.2.12. R-DS.2.2-2	34
6.2.13. R-DS.2.2-3	35
7. Spectroscopy	36
7.1. Applicable requirements.....	36
7.2. Instrumental configuration overview.....	37
7.3. Observational strategy overview.....	38
7.4. Optical parameters description and justification.....	38
7.4.1. Spectral bands.....	38
7.4.2. PSF evaluation.....	38
7.4.3. Resolution element evaluation	41
7.5. Instrument throughput evaluation	42
7.5.1. Instrument transmission	42
7.5.2. Telescope.....	42
7.5.3. Optical transmission	42
7.5.4. Detector quantum efficiency.....	42

7.5.5. Contamination and out of band transmission.....	43
7.5.6. Total transmission	43
7.6. Radiometric evaluation	44
7.6.1. Zodiacal noise.....	44
7.6.2. Detector noise	44
7.6.3. Other noise contributions.....	44
7.7. Other parameters	45
7.7.1. Number of operable pixels	45
7.7.2. Pixel response variation in one detector.....	45
7.7.3. Pixel size and plate scale.....	45
7.7.4. Gaps between detector	46
7.8. Observation parameters	46
7.8.1. Exposure time	46
7.8.2. Dithering strategy	46
7.8.3. Cosmic rays	46
7.9. Summary of parameters used for performance evaluation	47
7.10. Flux limit evaluation (GC.2.1-1 and GC.2.1.3)	48
7.10.1. Method.....	48
7.10.2. Results	50
7.11. The completeness/purity performance validation	55
7.11.1. Method and Tools	55
7.11.2. Impact of the quality of the image on the completeness.....	65
7.11.3. Completeness performance results with the full end to end pipeline	70
7.11.4. Inoperability of pixels	71
7.12. Spectroscopy level 1 requirements to NISP performance.....	72
7.12.1. Level 1 requirements.....	72
7.12.2. Results.....	73
7.12.1. Deep survey simulation.....	75
7.12.2. About zodiacal light	77
7.13. Future plan	78

List of Figures

Figure 1: The photon to electron conversion efficiency of the imaging mode on the NISP instrument, including contributions from the central obscuration, telescope, dichroic, NISP optics, photometry filters and detector quantum efficiencies. The coarse wavelength sampling of the reference dichroic transmission data leads to the discontinuities in the gradients at the wavelength extremes.	18
Figure 2, science impact: Relative change of photo-z outlier fraction, photo-z errors, and completeness from lower than required limiting sensitivity.....	29
Figure 3: Galaxy clustering relative sample completeness as a function of limiting sensitivity, relative to the requirement value of 24mag AB, for the Roche/Zamorani input catalog.	30
Figure 4: The sky coverage assuming a dithering strategy of (0'', 0''), (100'', 50''), (100'', 0''), (100'', 0'').	33
Figure 5: The 5σ detection limit in the deep field as a function of the number of visits. The observing mode in each visit is the same as for the wide survey.	34
Figure 6: the evolution of the PSF in function of the wavelength.....	41
Figure 7: Transmission for the spectroscopic channel.....	43
Figure 8: the number of pixel under the emission line in function of the object size convoluted with the PSF FWHM.....	51
Figure 9: Signal to noise function of the flux on the line for 2x560s exposure time for 2 assumption of the number of pixel under the emission line. the requirement (blue line) is to have SNR>3.5 sigma at 3 10-16 erg/cm ² /s.....	52
Figure 10: Signal to noise versus the exposure time. We see that we are just at the requirement for the blue band for 25 pixels and 2 exposures of 560s. There is clearly more margin in the red band.	52
Figure 11: Total detector noise integrated on 560s versus the QE of the detector, all other parameters are fixed as described in Table 26. The green points correspond to the 3 sigma limit and the functional region for science is almost a linear extrapolation under the green points.	53
Figure 12: Flux limit with the standard zodiacal value and using a higher value (2 X and 3X) of zodiacal for 3 cases of number of pixel under the emission line. This is done with pixel size of 0,3''	54
Figure 13: flux limit for a pixel size of 0,33'' and different number of pixel under the line.	55
Figure 14: a scheme of the end to end pipeline needed to test completeness and purity. In yellow are indicated information's coming from the instrument, in green current implementation of codes, light green when it is partly done and in white boxes what will be added in further steps.	57
Figure 15: Example of a simulated direct image (single array)	60
Figure 16: its dispersed counterpart in the blue band obtained with the aXeSIM software.....	60
Figure 17: example of de-contamination. Top: roll 0 observation, the object line is visible at 1.3m, while a much stronger line is visible at 1.7μ. Middle: roll 90 observation. The object line is (barely) visible at 1.3μ. Bottom, the combined spectrum. Comparison from the 2 rolls has allowed to flag the strongest line as a contaminant	62
Figure 18: example of spectrum affect by gaps in the roll 0 configuraton (top), but not in the roll 90 configuration (middle). The combined spectrum has a better S/N in the region observed in the two configurations.....	63
Figure 19; a simulated 1D spectrum with an H α emission line of $4 \cdot 10^{-16}$ erg/cm ² /s.....	64
Figure 20: A 1D simulated spectrum with an H α emission line of $8 \cdot 10^{-16}$ erg/cm ² /s. the Oiii line is also visible in this example on the left edge.	64
Figure 26; relative completeness on the blue band (left) and red band (right) when we vary the mean QE and noise RMS for all line $f > 1 \cdot 10^{-16}$ erg/cm ² /s and SNR>3.....	70
Figure 27 Completeness (top) and purity (bottom) evaluation using the current instrument and observational strategy implementation, for the three PSF cases WA, WW and WR (see text). The solid line indicates the current requirement, log-dashed line is the current goal. Error bars indicate purely poissonian fluctuations.	71

The presented document is Proprietary information of the Euclid Consortium.

This document shall be used and disclosed by the receiving Party and its related entities (e.g. contractors and subcontractors) only for the purposes of fulfilling the receiving Party's responsibilities under the Euclid Project and that the identified and marked technical data shall not be disclosed or retransferred to any other entity without prior written permission of the document preparer.

Figure 28: Left: difference between true and measured redshift as a function of the true one. The figures include all objects contributing to completeness. The dashed lines show the required 1sigma distribution.	74
Figure 29: The galaxy density distribution reconstructed with the end-to-end simulation with the current implementation for 2 PSF (average WA and reddest one WR). This distribution fulfills all requested Level 1 requirements.	75
Figure 30: deep survey simulations. Left: completeness and purity reached with 1 wide observation (black line), 6 wide-like observations (blue), 9 wide-like observations (green) and 12 wide-like observations (red). Right: real (black empty) and observed (red dashed) redshift distribution from the Deep survey. The top panel shows the difference between the mean redshift of the true distribution and the observed distribution.	76
Figure 31: redshift distribution obtained with a minimum zodiacal light as from requirement (left), with 2* minimal value (center) and with 3*minimal value (right)	77

List of Tables:

Table 1: A summary of the changes to the NISP Photometry requirements and flowdown	15
Table 2: Summary of the changes to the NISP Spectroscopy requirements between IPRR (AD1) and the SPR.....	16
Table 3: Parameters common to both operating modes of the NISP instrument used during the performance verification. The parameter are EO.....	17
Table 4: Parameters specific to the photometric mode of the NISP instrument used during the performance evaluation.	18
Table 5: Summary of specific spectroscopic parameters	19
Table 6: PSF description as EE50 + EE80 and as double Gaussian	21
Table 7: A summary of the Level 2 science requirements applicable to the NISP Photometry Mode (AD2)	21
Table 8: The budget breakdown of the dead pixel requirement.	22
Table 9: PSF comparison against requirements.....	24
Table 10: Relative photometric error budget allocations.....	26
Table 11: Comparison of ensquared energies of PSFs assumed in integration time calculations and actual PSF	27
Table 12: Mean S/N for 24 mag AB point sources in the nominal integration time.....	27
Table 13: Fraction of 24mag AB point sources with S/N<5 for different PSF and pixel scale cases in the 3 dither case. Given are the fractions for the different cases (columns 2-5) and the resulting total fractions under the assumptions of 50.9% of survey area covered with 4 dithers and 70% of FOV being covered by a WA and 30% by WW PSF. The bottom three rows show the same situation if through a mitigation process the signal is increased by ~25%, e.g. through longer integration times.....	28
Table 14: The exposure times (excl. readout overhead) per dither required to meet the NISP Photometry Mode's 5σ detection limit. Exposure times for the nominal case and a TBC modification are presented.....	31
Table 15: The Euclid mission's baseline dithering strategy.	32
Table 16: Summary of the sky coverage assuming a dithering strategy of $(0'', 0'')$, $(100'', 50'')$, $(100'', 0'')$, $(100'', 0'')$	33
Table 17: A summary of the number of visits to the deep required to meet the 5σ detection limit.	35
Table 18: Level 2 requirements for performance verification in spectroscopy.....	36
Table 19: instrument parameters for performance evaluation	37
Table 20: wide survey parameters for spectroscopy	38

Table 21: EEs values agree with ESA for average, worst cases for performance evaluation	39
Table 23: Parameters for the PSF evaluation in the worst case (WW).....	40
Table 24: dispersion per pixel for the 2 PSF (average and worst) cases considered in this study..	41
Table 25: telescope throughput	42
Table 26: Summary of spectroscopic instrument parameters used in simulation.....	48
Table 27: Spectroscopic Level 1 requirement validation. Items marked with * are verified through deep survey simulations.....	72
Table 28: galaxy density, completeness and purity as a function of zodiacal light.....	77

The presented document is Proprietary information of the Euclid Consortium.

This document shall be used and disclosed by the receiving Party and its related entities (e.g. contractors and subcontractors) only for the purposes of fulfilling the receiving Party's responsibilities under the Euclid Project and that the identified and marked technical data shall not be disclosed or retransferred to any other entity without prior written permission of the document preparer.

1. Purpose and Scope

This document validates the performance of the NISP instrument against the Euclid Level 2 Science Requirements detailed in the Science Requirement Document (AD1).

The baseline instrument parameters used in the performance verifications are summarized in Section 5. Parameters common to both instrument operating modes are tabulated in Section 5.1, followed by the photometric mode specific parameters and the spectroscopic mode specific parameters in Sections 5.2 and 5.3 respectively.

Section 6 describes the performance verification of the requirements applicable to the photometric mode of the instrument and Section 7 describes the verification done for the spectroscopic mode. For the spectroscopic mode some Level 1 Science Requirements verification will also be presented.

The presented document is Proprietary information of the Euclid Consortium.

This document shall be used and disclosed by the receiving Party and its related entities (e.g. contractors and subcontractors) only for the purposes of fulfilling the receiving Party's responsibilities under the Euclid Project and that the identified and marked technical data shall not be disclosed or retransferred to any other entity without prior written permission of the document preparer.

2. Documents

2.1. Applicable documents

AD	Title / Author	Document Reference	Issue	Date
AD1	Euclid Science Requirements Document / R. Laureijs (ESA)	DEM-SA-Dc-00001	5.2	20/08/11
AD2	Euclid System performance budget documents (SPBD)	SRE-PA/2011.00..	2	15/05/11
AD3	Euclid Payload Element Requirement Document (PERD) / L. Duvet (ESA)	SRE-PA/2011.006	2	26/10/11
AD4	Mission requirement document (MRD)	SRE-PA/2010.025	3	26/10/2011
AD5	Detector specifications	SRE-PA/2011.032	4	19/10/2011
AD6	Limiting sensitivity analysis NISP photometry P.Ferruit	TN00007	4	28/10/11

2.2. Reference documents

2.2.1. Euclid Project Reference Document.

RD	Title / Author	Document Reference	Issue	Date
RD1	NISP Calibration Plan	EUCL-MPI-NPS-PL-00078	1.0	19/05/11
RD2	Technical Note on the PSF-spectral dispersion	EUCL-NISP-TN-04	1.0	18/03/11
RD3	TN on NISP NI-DCU	EU-NISP-TN-xxx	1.0	14/04/11
RD4	TN on NISP NI-CU Intensity of fiber-fed flat-fielding	EU-NI-CU-MPIA-TN002_1_0	1.0	10/05/11
RD5	NI-OMA Design Definition Report	EUCL-LAM-NPS-RP-00093	1.0	
RD6	NI-OMA Design Justification Report	EUCL-SIS-NPS-ADD-00046	1.0	06/05/11
RD7	NISP Technical Specifications	EUCL-SIS-NPS-DVP-00045	1.0	06/05/11
RD8	Ni-DS Design Report	EUCL-SIS-NPS-DVP_00048	1.0	06/05/11
RD9	EEs NISP spectroscopy justification	EUCL-CPP-NPS-TN-00208	1.0	11/01/12
RD10	Mission performance document	EUCL-IAP-EUC-DP-00244	1	15/01/12

The presented document is Proprietary information of the Euclid Consortium.

This document shall be used and disclosed by the receiving Party and its related entities (e.g. contractors and subcontractors) only for the purposes of fulfilling the receiving Party's responsibilities under the Euclid Project and that the identified and marked technical data shall not be disclosed or retransferred to any other entity without prior written permission of the document preparer.

2.2.1. ECSS Reference Documents.

RS	Title / Author	Document Reference	Issue	Date
1	Space Project Management: Project Planning and Implementation	ECSS-M-ST-10C	-	06/07/09
2	Space Project Management: Configuration and Information Management	ECSS-M-ST-40C	-	06/07/09
3	Space Project Management: Cost and Schedule Management	ECSS-M-ST-60C	-	31/07/08
4	Space Project Management: Risk Management	ECSS-M-ST-80C	-	31/07/08
5	Space Project Engineering: Software engineering	ECSS-E-ST-40	-	06/07/09
6	Space product assurance discipline: Software product assurance	ECSS-Q-ST-80	-	06/07/09

The presented document is Proprietary information of the Euclid Consortium.

This document shall be used and disclosed by the receiving Party and its related entities (e.g. contractors and subcontractors) only for the purposes of fulfilling the receiving Party's responsibilities under the Euclid Project and that the identified and marked technical data shall not be disclosed or retransferred to any other entity without prior written permission of the document preparer.

3. Acronyms

Q	As Build Configuration List	EOL	End Of Life
ACS	Advanced Camera for Survey	EPLM	Euclid Payload Module
AD	Applicable Document	ESA	European Space Agency
ADC	Analog to Digital Converter	ESST	Euclid Science Study Team
ADU	Analog to Digital Unit	ESVM	Euclid Service Module
AIT	Assembly Integration and Test	ETC	Exposure Time Calculator
AV	Assembly Integration and Verification	FAR	Flight Acceptance Review
AO	Announcement of Opportunity	FDIR	Failure Detection Isolation and Recovery
AOCS	Attitude and Orbit Control System	FE	Front End
AR	Acceptance Review (instruments)	FEM	Finite Element Model
AR	Anti-Reflection	FGS	Fine Guidance Sensor
ASI	Agenzia Spaziale Italiana	FM	Flight Model
ASIC	Application Specific Integrated Circuit	FMEA	Failure Mode Effects Analysis
ATC	Astronomy Technology Centre	FOV	Field Of View
BAO	Baryonic Acoustic Oscillation	FP	Focal Plane
BOL	Beginning Of Life	FPA	Focal Plane Assembly
BSP	Board Support Package	FPE	Focal Plane Electronics
CAD	Computer Aided Design	FPGA	Field Programmable Gate Array
CaLA	Camera Lens Assembly	FSM	Finite State Machine
CCD	Charge coupled device	FW	Flight Wheel
CDF	Concurrent Design Facility	FWA	Filter Wheel Assembly
CDMS	Command and Data Management System	FWHM	Full Width Half Maximum
CDMU	Command and Data Management Unit	GND	Ground
CDPU	Control and Data Processing Unit	GSE	Ground Support Equipment
CDR	Critical Design Review	GWA	Grim Wheel Assembly
CEA	Commissariat à l'Energie Atomique	H2RG	HAWAII 2RG (HgCdTe Astronomy Wide Area Infrared Imager 2k2 Resolution, Reference pixels and Guide mode)
CFHTLS	Canada-France-Hawaii Telescope Legacy Survey	HDR	Hardware Design Review
CI	Configuration Item	HgCdTe	Hg (Mercury) Cadmium Telluride
CIDL	Configuration Item Data Lists	HK	House keepings
CM	Cryo Mechanism	HST	Hubble Space Telescope
CMU	Compensating Mechanism Unit (=NI-CMU)	I/F	Interface
CMD	Command	I/O	Input Output
CMOS	Complementary Metal Oxide Silicon	IAS	Institut d'Astrophysique Spatiale
CMRR	Common Mode Rejection Ratio	IASF-Bo	INAF Istituto di Astrofisica Spaziale Bologna
CNES	French Space National Agency	IBDR	Instrument Baseline Design Review
CoG	Center of Gravity	ICD	Interface Control Document
CoLA	Corrector Lens Assembly	ICE	ICE
CPPM	Centre de Physique des Particules de Marseille	ICU	Instrument Control Unit
CPU	Central Processing Unit	IEEC	Institut d'Estudis Espacials de Catalunya
CSIC	CSIC	INAF	Istituto Nazionale AstroFisica
CSS	Cold Support Structure (of NI-DS)	IOT	Instrument Operation Team
CTE	Coefficient of Thermal Expansion	IPRR	Instrument Preliminary Readiness Review
DLL	Design Limit Load	IQR	Instrument Qualification Review
DAC	Digital to Analog Converter	IRFU	Institut de Recherche sur les lois Fondamentales de l'Univers - CEA
DARK	Dark Cosmology Centre (Denmark)	IRR	Instrument Requirement Review
DIT	Detector Integration Time	ISO	International Organization for Standardization
DPU	Data Processing Unit	IT-Ind	Italian Industry
DQE	Detective Quantum Efficiency	JLP	Jet Propulsion Laboratory
DTCP	Daily Telemetry Communications Period	LAM	Laboratoire d'Astrophysique de Marseille
DTU	Denmarks Tekniske Universitet	LET	Linear Energy Transfer
EC	Euclid Consortium	LLD	Launch Lock Device
ECSS	European Cooperation for Space Standardization	LLI	Long Lead Item
EE	Encircled Energy	LSB	Least Significative Bit
EGSE	Electrical Ground Support Equipment	LSF	Least Square Fit
EIC	Euclid Imaging Channels	LVDS	Low Voltage Differential Signal
EID	Experiment Interface Document	MACC	Multi Accumulation Readout
EIR	Euclid Instrument Requirement	MCT	Mercury Cadmium Telluride
ELM	Euclid Legacy Archive	MGSE	Mechanical Ground Support Equipment
EM	Electrical Model	MIPS	Mega Instructions Per Second
EMA	Euclid Mission Archive	PSU	Power Supply Unit
MLI	Multi layer Insulation	QE	Quantum Efficiency
MMU	Mass-Memory Unit	RD	Reference Document
MOC	Mission Operations Centre	RFA	Request For Approval
MOGS	Mission Operations Ground Segment		

The presented document is Proprietary information of the Euclid Consortium.
 This document shall be used and disclosed by the receiving Party and its related entities (e.g. contractors and subcontractors) only for the purposes of fulfilling the receiving Party's responsibilities under the Euclid Project and that the identified and marked technical data shall not be disclosed or retransferred to any other entity without prior written permission of the document preparer.

Mol	Moment of Inertia
MOU	Memorandum Of Understanding
MPE	Max Planck institut für Extraterrestrische physik
MPIA	Max Planck Institut für Astronomie
MRD	Mission Requirement Document
MSSL	Mullard Space Science Laboratory
N/A	Not Applicable
NCR	Non Conformance Request
NDRO	Non Destructive Readout
NI-CMU	NISP Compensation Mechanism Unit
NI-CU	NISP Calibration Unit
NI-DCU	NISP Detector Control Unit
NI-DPU	NISP Data Processing Unit
NI-DS	NISP Detection System
NI-FPA	NISP Focal plane Assembly
NI-FWA	NISP Filter Wheel Assembly
NI-GWA	NISP Grism Wheel Assembly
NI-HSS	NISP Harness
NI-HSS-IU	NISP Inter Unit Harness
NI-HSS-TH	NISP Thermal Harness
NI-ICU	NISP Instrument Control Unit
NI-OA	NISP Optics Assembly
NI-OMA	NISP Opto Mechanical Assembly
NIP	Near Infrared Photometry
NIR	Near Infrared
NIS	Near Infrared Spectrograph
NI-SA	NISP Structure Assembly
NI-SCS	NISP Sensor Chip System
NISP	Near Infrared Spectrometer and Photometer
NI-TC	NISP Thermal Control
NI-WE	NISP Warm Electronics
NPM	National Project Manager
NRB	Non-conformance Review Board
OABr	INAF Osservatorio Astronomico di Brera
OAPd	INAF Osservatorio Astronomico di Padova
OATo	INAF Osservatorio Astronomico di Torino
OBSW	On Board Software
OGSE	Optical Ground Support Equipment
OSTM	Optical and Structural and Thermal Model
OTE	Optical Telescope Element
PA	Product Assurance
PA/QA	Product Assurance / Quality Assurance
PAP	Product Assurance Plan
PCB	Printed Circuit Board
PCE	Photon to electron Conversion Efficiency
PDD	Payload Definition Document
PDR	Preliminary Design Review
PERD	Payload Element Requirement Document
PI	Principal Investigator
PID	Proportional Integral Derivative
PLM	PayLoad Module
PM	Project Manager
PMCU	Parameters and Mechanism Control Unit
PMP	Project Management Plan
PN	Planetary Nebulae
PRTECH	Prototech
PS	Project Scientist
PSF	Point Spread Function

RMS	Root Mean Square
RMW	Read Modify Write
ROI	Region Of Interest
ROIC	Readout Integrated Circuit
ROM	Rough Order of Magnitude
RON	ReadOut Noise
RTD	Resistance Temperature Device
S/C	Spacecraft
SAA	Solar Aspect Angle
SAp	Service d'Astrophysique – CEA/IRFU
SCA	Sensor Chip Assembly
SCE	Sensor Chip Electronic
SciRD	Science Requirement Document
SDC	Science Data Center
SED	Single Event Damage
SEL	Single Event Latch-up
SEU	Single Event Upset
SFR	Star Formation Rate
SGS	Science Ground Segment
SiC	Silicon Carbide
SIDECAr	System for Image Digitization, Enhancement, Control And Retrieval.
SIS	Service d'Ingénierie des Systèmes – CEA/IRFU
SLI	Single Layer Insulation
SMM	Structural Mathematical Model
SNR	Signal to Noise Ratio
SOC	Science Operation Center
SPC	Science Program Committee
SPW	Space Wire
SSC	Space Science Center (Denmark)
STM	Structure & Thermal Model
SVM	Service module
SWL	Space Wire Link
TA	Telescope Assembly
TBC	To Be Confirmed
TBD	To Be Defined
TBV	To Be Verified
TBW	To Be Written
TC	Telecommand
TCS	Thermal Control System
TE	Test Equipment
TGSE	Thermal Ground Support Equipment
TIF	Thermal Inter Face
TIS	Teledyne Imaging Sensors
TLM	Telemetry
TM	Telemetry
TMA	Three Mirrors Anastigmat
TN	Technical Note
TOp	Temperature Operating
TRL	Technology Readiness Level
TT&C	Telemetry, Tracking and Command
UPCT	Technical University of Cartagena
URF	Unit Reference Frame
UTR	Up The Ramp Readout
VIS	VISIBLE Instrument
WE	Warm Electronics
WFC3	HST Wide Field Camera 3
WFE	Wave Front Error
WL	Weak Lensing
WP	Work Package
WPD	Work Package Description

The presented document is Proprietary information of the Euclid Consortium.

This document shall be used and disclosed by the receiving Party and its related entities (e.g. contractors and subcontractors) only for the purposes of fulfilling the receiving Party's responsibilities under the Euclid Project and that the identified and marked technical data shall not be disclosed or retransferred to any other entity without prior written permission of the document preparer.

4. Requirement flow down and verification

During the Phase A2 study the Euclid science requirements have been reinvestigated, with modifications and new justifications applied for some requirements. Now, the L2 requirements are flown down to lower levels through the different ESA applicable documents: The SPBD (AD2) will separate the contribution of the instrument, telescope, mission and ground segment. The PERD document (AD3) will list the requirements, which are now applicable to the instrument. The MRD document will list requirement at telescope or satellite level (AD4).

In this Performance Analysis Report we validate the performance of the NISP instrument against the Level 2 requirements stated in the ESA Science Requirement Document (AD1) and flown down through AD2 to AD3 and AD4. Table 1 and Table 2 detail the L2 requirement flow down details and the need for modification from the current version of documents.

4.1. Photometry Requirement Modifications

Reference	No Change	Direct PERD	SPPBD	Requirement Summary	Description of Change
R-WL.2.1-12		X	X	Stray light surface brightness	Removed; now L3 requirement only, flowing from limiting sensitivity
R-WL.2.1-13	X	X		Fraction of pixels lost to permanently dead pixels and cosmics (per frame)	Relaxed from 5% to 10% in the NISP and now includes dead pixels. The original justification for the requirement (from calibration) was only applicable to the VIS instrument.
R-WL.2.1-17	X	X		Wavelength Range (out of band transmission)	
R-WL.2.1-18	X	X		Number of bands	
R-WL.2.1-19			X	System PSF Size	Now expressed in EE50 and EE80 instead of FWHM. Requirements added in Y and H bands. Also, the values given only apply to the effect of crowding and represent maximal limits. More stringent limits flow from the survey depth but can be traded off with integration time.
R-WL.2.1-20	X			Pixel Scale	Set to a fixed value with a tolerance.
R-WL.2.1-21	X			Post Calibration Relative Photometric Error (goal)	Earlier relaxed from < 0.5% to < 1.5 %. Simulations had shown that the original requirement was unnecessarily stringent.
R-WS.2.2-3	X			Wide Survey Magnitude Limit	AB 24 (5σ , point source)
R-WS.2.2-6	X			Numbers of dithers in VIS and NISP	Minimal area coverage was removed earlier on, now just stated that the survey must be performed with 4 dithers.
R-WS.2.2-7	X			Fraction of pixels seeing 3 dithers	Relaxed from > 95% to > 92%. The old requirement is infeasible with available detector mosaics.
R-WS.2.2-10		X		Image depth for spectroscopy association	Image depth now specified as AB 24 (5σ , point source), not for extended sources anymore
R-DS.2.2-2	X			Deep Survey Magnitude Limit	
R-DS.2.2-3	X			Deep Survey Depth per Visit	

Table 1: A summary of the changes to the NISP Photometry requirements and flowdown

The presented document is Proprietary information of the Euclid Consortium.

This document shall be used and disclosed by the receiving Party and its related entities (e.g. contractors and subcontractors) only for the purposes of fulfilling the receiving Party's responsibilities under the Euclid Project and that the identified and marked technical data shall not be disclosed or retransferred to any other entity without prior written permission of the document preparer.

4.2. Spectroscopic Requirements and modifications for PERD

Reference	No Change	Direct PERD	SPBD	Requirement Summary	
GC.2.1-1	x		x	Flux limit	
GC.2.1-2	x		x	Completeness	-
GC.2.1-3	x		x	Variation in Flux limit vs. wavelength	
GC.2.1-4	x	x		Spectral range limits	
GC.2.1-5			x	Spectral resolution	
GC.2.1-6	x			Resolution element	-
GC.2.1-7	x			Wavelength error	-
GC.2.1-8			x	PSF size and shape in spectroscopic mode	Suppressed flown from SPBD
GC.2.1-9			x	Stray light	To be suppress flown from SPBD
GC.2.1-10				Pure Sample	
WS.2.2-6				Number of dither	
WS.2.2-7	x			Dither strategy	
WS.2.2-8	x			Spectro observation strategy	

Table 2: Summary of the changes to the NISP Spectroscopy requirements between IPRR (AD1) and the SPR.

The presented document is Proprietary information of the Euclid Consortium.

This document shall be used and disclosed by the receiving Party and its related entities (e.g. contractors and subcontractors) only for the purposes of fulfilling the receiving Party's responsibilities under the Euclid Project and that the identified and marked technical data shall not be disclosed or retransferred to any other entity without prior written permission of the document preparer.

5. Instrument Configuration

In this section we detail the baseline instrument configuration used during the performance verification for the SPR highlighting the difference with the evaluation done in RD4. In Section 5.1, parameters common to both of the instrument's operating modes are tabulated. In Sections 5.2 and 5.3 the parameters relevant on to the Photometric and Spectroscopic modes respectively are tabulated.

5.1. Common Parameters

The parameters common to both the NISP photometric and spectroscopic science modes are shown in Table 3.

Parameter	Value	Reference
Telescope		
Main Mirror Radius	60 cm	AD4
Central Obscuration	11 %	AD4
AOCS PSF	Gaussian, FWHM = 3 μm	AD4
Dithering Strategy	Dither 1: X=0'', Y=0'' Dither 2: X=100'', Y= 50'' Dither 3: X=100'', Y= 0'' Dither 4: X=100'', Y= 0''	AD4
Instrument		
Temperature (NIOMA)	140 K	RD5
Focal Plane		
Pixels per Detector	2040×2040	AD5
Active Area	36.72×36.72 mm	AD5
Number of Detectors	4×4	AD3
Gaps between Detectors	3×6 mm	AD3
Quantum Efficiency	0.7	AD5
Gain	1	AD5
Detector PSF	Gaussian, FWHM = 4 μm	
Detector Cut-off	2.4 μm	AD5

Table 3: Parameters common to both operating modes of the NISP instrument used during the performance verification. The parameter are EO

5.2. Photometry Specific Parameters

The parameters specific to the NISP Photometry Mode are shown in Table 3.

Parameter	Value	Reference
Optics		
Photon to Electron Conversion Efficiency	See Figure 1	RD3
Pixel Scale	0.3''/0.33''	RD3
Optical PSF	Polychromatic PSFs from the	RD3

	reference toleranced optical design expressed in EE50, EE80, combined with integration error and expressed into double Gaussian	
Focal Plane		
Total noise	7.7 e ⁻ rms	EOL, compliant with the total noise requirement in RD8
Dark Current	0.1 e ⁻ s ⁻¹ pix ⁻¹	
Universe Parameters		
Sky Background Surface	Y = 22.09 (AB) J = 22.07 (AB) H = 22.20 (AB)	RD3
Sky Background at Ecliptic Pole	Y = 22.69 (AB) J = 22.67 (AB) H = 22.80 (AB)	RD3

Table 4: Parameters specific to the photometric mode of the NISP instrument used during the performance evaluation.

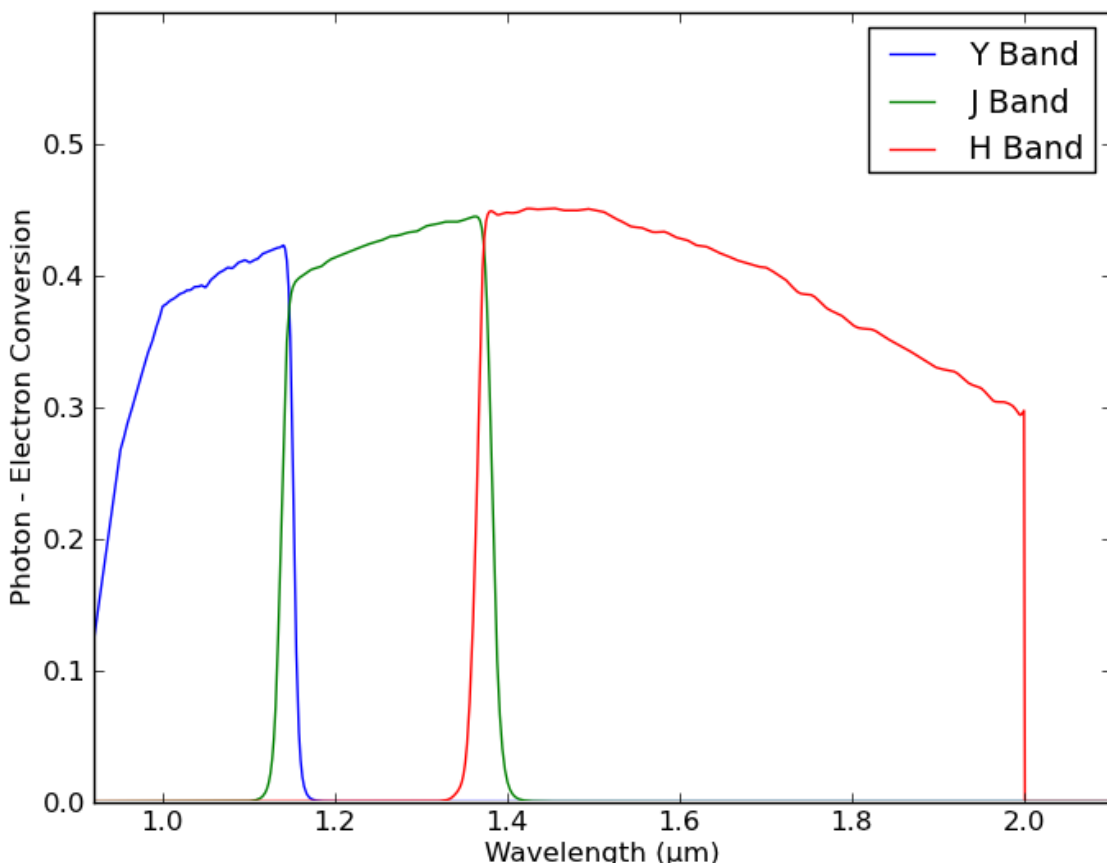


Figure 1: The photon to electron conversion efficiency of the imaging mode on the NISP instrument, including contributions from the central obscuration, telescope, dichroic, NISP optics, photometry filters and detector quantum efficiencies. The coarse wavelength sampling of the reference dichroic transmission data leads to the discontinuities in the gradients at the wavelength extremes.

The presented document is Proprietary information of the Euclid Consortium.
 This document shall be used and disclosed by the receiving Party and its related entities (e.g. contractors and subcontractors) only for the purposes of fulfilling the receiving Party's responsibilities under the Euclid Project and that the identified and marked technical data shall not be disclosed or retransferred to any other entity without prior written permission of the document preparer.

5.3. Spectroscopy Specific Parameters

The spectroscopic specific parameters are summarized In Table 5. Details will be given in section 7.

Parameter	Value	Compliance ref
Grism bands (nm)	Blue=1100-1457 Red=1445-2000	RD3 R-NIS-F-012
Out of band	10-3	RD3 R-NIS-P-002
Dispersion/pixel	9.8A/pix	RD3 R-NIS-P-003
transmission	See curve Instrument telescope	RD3 R-NIS-P-001 R-6231-6
Optical PSF EE in radius (asec) average	Double Gaussian Blue EE50= 0,18'' EE80 = 0,45'' RedEE50=0,22'' EE80 = 0,57''	RD3 R-NIS-P-008
Detector PSF	4 nm	
noise (instrument entrance)	Blue = $1 \text{ e s}^{-1} \text{ pix}^{-1}$ Red = $0,99 \text{ e s}^{-1} \text{ pix}^{-1}$	RD2 SPBD
Instrument noise	Blue < $0,093 \text{ e s}^{-1} \text{ pix}^{-1}$ Red < $0,093 \text{ e s}^{-1} \text{ pix}^{-1}$	RD3 R-NIS-P-007
Scatter light noise	Blue < $0,1 \text{ e s}^{-1} \text{ pix}^{-1}$ Red < $0,1 \text{ e s}^{-1} \text{ pix}^{-1}$	RD2 R-6232-8
Exposure time	560s	R-NIS-F-009

Table 5: Summary of specific spectroscopic parameters

The presented document is Proprietary information of the Euclid Consortium.

This document shall be used and disclosed by the receiving Party and its related entities (e.g. contractors and subcontractors) only for the purposes of fulfilling the receiving Party's responsibilities under the Euclid Project and that the identified and marked technical data shall not be disclosed or retransferred to any other entity without prior written permission of the document preparer.

6. Photometric Mode

6.1. Point Spread Function

PSFs have been constructed in each band (YJHBR) from:

1. Polychromatic optical PSFs, produced from the reference 95% tolerated optical system at the 9 field points used during the optical optimizing (see RD5 and RD6).
2. An AOCS PSF, modeled as a Gaussian PSF with a FWHM of 3 μm . This model is consistent with the AOCS time series provided by the two industries.
3. A detector PSF, modeled as a Gaussian PSF with a FWHM of 4 μm . This accounts for detector effects, such as cross talk and interpixel capacitance.
4. As agreed with ESA the PSFs are expressed in terms of EE50 and EE80 only.
5. In quadrature the effects of integration have been added to EE50 and EE80, which represents a conservative approach
6. Three PSFs are extracted from this procedure: i) The average PSF over the FOV (WA PSF), ii) the worst PSF over the FOV (WW PSF) and iii) a worst over the FOV + 10% PSF (WW10).
7. In order to allow the use in numerical simulations and in the absence of a PSF shape, these PSFs are expressed in terms of double Gaussians. In order to convert the two-parameter PSFs (EE50+EE80) into a three-parameter Gaussian (σ_1 , σ_2 and relative intensity c_1) it was assumed that EE90=2xEE80. With these numbers the PSF representations in Table 6 were calculated.

	Y	J	H	B	R
WA PSF					
EE50 ["]	0.18	0.18	0.20	0.18	0.22
EE80 ["]	0.38	0.43	0.57	0.45	0.57
EE90 ["]	0.76	0.86	1.14	0.90	1.14
σ_1 ["]	0.12558	0.123755	0.136376	0.123389	0.150535
σ_2 ["]	0.575815	0.636714	0.838874	0.664314	0.840262
c_1	0.985287	0.987631	0.991185	0.98861	0.989358
WW PSF					
EE50 ["]	0.29	0.30	0.31	0.3	0.32
EE80 ["]	0.53	0.53	0.62	0.55	0.63
EE90 ["]	1.06	1.06	1.24	1.1	1.26
σ_1 ["]	0.211476	0.222874	0.218814	0.218437	0.226849
σ_2 ["]	0.916218	1.01024	0.963599	0.94468	0.989831
c_1	0.987238	0.989894	0.984926	0.987055	0.984994
WW10 PSF					
EE50 ["]	0.32	0.33	0.34	0.33	0.35
EE80 ["]	0.58	0.58	0.68	0.61	0.69
EE90 ["]	1.17	1.17	1.36	1.21	1.39
σ_1 ["]	0.234446	0.246051	0.239989	0.239224	0.248184
σ_2 ["]	1.03438	1.14406	1.05685	1.01948	1.09397

c ₁	0.988125	0.990702	0.984926	0.986233	0.985347
----------------	----------	----------	----------	----------	----------

Table 6: PSF description as EE50 + EE80 and as double Gaussian

Please also see 7.4.2 for more information.

6.2. Applicable Requirements

The Level 2 science requirements applicable to the NISP Photometry mode are summarized in Table 7.

Reference	Description	Requirement	Compliant?
R-WL.2.1-12	Stray light surface brightness	< 20 % zodiacal at ecliptic pole	Removed, now L3
R-WL.2.1-13	Fraction of lost pixels (dead and glitches)	< 10 %	Inoperable pixels: ✓ CR hits/glitches: Verification ongoing
R-WL.2.1-17	Wavelength Range (out of band transmission)	920 – 2000 nm (10^{-4})	✓
R-WL.2.1-18	Number of bands	≥ 3	✓
R-WL.2.1-19	System PSF Size from confusion limit: EE50 (EE80)	< 0.4'' (<0.7'') (any band)	✓
R-WL.2.1-20	Pixel Scale	0.300'' +/- 0.03	✓
R-WL.2.1-21	Post Calibration Relative Photometric Error	< 1.5 %	✓
R-WS.2.2-3	Wide Survey Detection Limit	AB 24 (5 σ)	✓ ✗ (wider PSF)
R-WS.2.2-6	Number of survey dithers	4	✓
R-WS.2.2-7	Percentage of wide survey covered in at least 3 dithers	> 90 %	✓
R-WS.2.2-10	Image depth for spectroscopy association	AB 24 (5 σ)	✓ ✗ (wider PSF)
R-DS.2.2-2	Deep Survey Magnitude Limit	DS + 2 mag	✓
R-DS.2.2-3	Deep Survey Depth per Visit	AB 24 (5 σ)	✓ ✗ (wider PSF)

Table 7: A summary of the Level 2 science requirements applicable to the NISP Photometry Mode (AD2)

6.2.1. R-WL.2.1-12

The diffuse stray light surface brightness in the VIS and NISP shall be less than 20% of the ecliptic pole zodiacal light.

This requirement has been removed from L2 and is now an L3 requirement flowing from the limiting sensitivity requirements (R-WS.2.2-3, R-WS.2.2-10, R-DS.2.2-3). Hence no

The presented document is Proprietary information of the Euclid Consortium.

This document shall be used and disclosed by the receiving Party and its related entities (e.g. contractors and subcontractors) only for the purposes of fulfilling the receiving Party's responsibilities under the Euclid Project and that the identified and marked technical data shall not be disclosed or retransferred to any other entity without prior written permission of the document preparer.

performance verification is required here but this only enters a L3 into the limiting sensitivity demonstration.

6.2.2. R-WL.2.1-13

The fraction of pixel lost due to glitches (including cosmic rays) and dead pixels in each exposure/frame shall be less than 2% in VIS and 10% in NISP.

Goal: The fraction of pixel lost due to glitches (including cosmic rays) in each exposure/frame shall be less than 1% in VIS and 5% in NISP.

There are two main contributors to this requirement, they are:

- (i) the detector dead/inoperable pixels and
- (ii) the pixels lost per frame due to cosmic ray hits

The budget breakdown of this requirement is shown in Table 8.

Contributor	Budget Allocation	Compliant
Dead/inoperable Pixels (EOL)	8 %	yes
Pixels lost to cosmic ray events per frame	2 %	Verification ongoing

Table 8: The budget breakdown of the dead pixel requirement.

The dead pixel (EOL) requirement (92% operability) is a non-trivial number. It is a combination of truly dead or hot pixels, but also includes the effect of pixels with a substantially lower performance due to either high noise, or low quantum efficiency, or both. The explanation T-WL.1.2-13 also goes beyond simple missing pixels: “*For the NISP the requirement comes from the worst-case scenario where a galaxy image is lost in all exposures and photometry is not available for photometric redshifts.*” Hence the 92% refer to lost galaxies and not lost pixels.

This leads to a re-assessment of this requirement and separates it into two further parts: i) Truly dead/hot pixels, ii) sub-average performing pixels. Since sub-average pixels still generate finite S/N they should not be discarded, but an operability criterion should be instated in terms, e.g. of S/N or weight delivered by a single pixel that can be used to assess which effective weight the pixels have on which a particular galaxy falls and whether this weight is particularly low.

Hence the 92% operability requirement needs to be interpreted defining a maximum number of really inoperable dead/hot pixels at EOL. The remainder between actually inoperable pixels and 100%-92%=8% can then be used to remove additional galaxies with the lowest weights from the observations, in order to decrease the number of low S/N galaxies.

The maximum number of dead pixels has been specified to the vendor and they are compliant with a guarantee of <4% of inoperable pixels, with “operability” defined as QE>35% and CDS readnoise <50e⁻ and dark current (100K) <1e⁻/s/pix. While we have no time degradation number to estimate EOL, the factor of 2 makes us confident that we are compliant with the 92% operability budget.

Since the impact of shielding around the instrument is not finalized, it is not possible to validate the requirement on the number of pixels lost to cosmic ray events. This budget allocation is therefore applied as an implicit requirement on the detector shielding and the impact of nominal shielding has to be finalized. Even though this is ongoing, a budget allocation of 2% is not seen as critical and we expect the performance to meet the requirement.

6.2.3. R-WL.2.1-17

The NISP imaging wavelength coverage shall have a min cut off of 920 nm and maximum cut off greater than 1600nm, where the off band transmission is less than 10^{-4} .

Goal: The NISP imaging wavelength coverage shall have a min cut off of 920 nm and maximum cut off greater than 2000nm, where the off band transmission is less than 10^{-4} .

The photon-to-electron photon conversion efficiency of the NISP imaging mode is shown in Figure 1. The instrument is sensitive in the wavelength range at least 920 – 2000 nm, with the short and long wavelength cutoffs given by Y-filter+dichroic (blue end) and H-filter (red end) and therefore the goal here is met. The off-band transmission requirement can be met with the photometry filters; these have an off-band transmission specified as $< 10^{-4}$. This is feasible with current filter technology (see RD5).

This requirement is met with the baseline instrument design.

6.2.4. R-WL.2.1-18

The NISP photometric channel shall have 3 or more bands.

Additional Text: For example Y (920-1146nm), J(1146-1372nm), and H(1372-1600nm) or H(1372-2000nm). These bands provide good synergy with ground based survey complement to meet the photometric redshift requirements. Further optimization may be possible.

The baseline design of the NISP instrument incorporates three photometry filters matching those suggested (see RD5). Mechanism, volume and survey constraints do not allow more.

This requirement is met with the baseline instrument design.

6.2.5. R-WL.2.1-19

The radii Encircling 50% of Energy (rEE50) and 80% of Energy (rEE80) shall be lower than 0.4 arcseconds and 0.7 arcseconds respectively for all wavelengths below 1486 nm.

PSF construction is described in Section 6.1. The three PSFs (WA, WW, WW10) are compared with the requirements in and is compliant with this requirement.

Units: arcsec	requirement	actual Y	actual J	actual H	Compliant?
WA EE50	< 0.4	0.18	0.18	0.20	✓
WA EE80	< 0.7	0.38	0.43	0.57	✓
WW EE50	< 0.4	0.29	0.30	0.31	✓

WW EE80	<0.7	0.53	0.53	0.62	✓
WW10 EE50	<0.4	0.32	0.33	0.34	✓
WW10 EE80	<0.7	0.58	0.58	0.68	✓

Table 9: PSF comparison against requirements**6.2.6. R-WL.2.1-20**

The pixel scale of NISP in imaging mode shall be 0.3 ± 0.030 arcsec.

This requirement is split into two parts: (i) the absolute value of the pixel scale and (ii) the variation of the pixel scale across the field of view.

The absolute value of the imaging mode's pixel scale is measured at the center of the focal plane. Assuming an $18 \times 18 \mu\text{m}$ pixel, the values here are $0.300''$, $0.300''$ and $0.300''$ (to 3 significant figures) in the Y, J and H bands respectively. The absolute requirement on the pixel scale is therefore met.

Two effects result in a variation of the pixel scale across the field of view:

- i. the optical distortion and
- ii. the variation in pixel sizes

The photometry mode of the NISP instrument has a low optical distortion in all bands ($< 2.5\%$ RD6). The variation in pixel scale due to the optical distortion is roughly an order of magnitude less than this tolerance. The dominant effect is therefore the variation in pixel sizes over the field of view. The detector pixels are specified (RD8) to have a size of $18 \pm 1 \mu\text{m}$. Assuming a constant plate scale of $0.3''/18 \mu\text{m} = 0.0166''/\mu\text{m}$, this $\pm 1 \mu\text{m}$ size variation translates to a $\pm 0.0166''$ variation in the pixel scale. Even with the worst case assumption that the biggest variation in pixel sizes is at the positions of highest distortion, this tolerance is still met.

This requirement is met in all bands.

6.2.7. R-WL.2.1-21

The post calibration relative photometric error in NISP imaging shall be less than 1.5%.

Goal: The post calibration relative photometric error in NISP imaging shall be less than 1.0%.

This requirement is broken down into a budget for different components. The first breakdown level and derived calibration procedures are detailed in the NISP Calibration Plan (RD1). Here we show a new breakdown to lower allocation levels, detailed below. This budget is complete and the requirement is met.

In progress is an assessment of the full set of the actual allocations on lower levels. For some entries information from JWST NIRcam can already be referenced. Discussions have been initiated for all allocations, also for those where NIRcam references exist, which could lead to a

redistribution of the individual allocations. E.g. since the PSF has grown broader with respect to what was assumed so far for the calculation of the impact of intra-pixel sensitivity variation, this effect will decrease and could become negligible which was already predicted for the red-end of the NISP wavelength coverage and the previous PSF. A second example is the impact of fringing. TIS has made a statement that this is not affecting NISP observations, even though NIRcam, using similar detectors, has a budget allocated for fringe flats and fringe flat stability. This needs added discussion. We have kept a budget allocation for this case but it might not be needed in the end.

When these discussions have fully stabilized the budgeting at lower allocation levels, we will make, if required, request for necessary changes to GDPRD and/or Calibration Plan on knowledge or performance requirements, as well as updates to the SPBD. We expect these changes to be small.

Allocation Levels									
	Top	A	B	C	D	Unit	E	Estimated	Justification/Comment
Top Level NISP-P Imaging Flux Calibration Accuracy	1.50								
Margin		0.29							
Subtotal		1.47							
Spat. PSF var. Error		0.60							
Calibration Stability		0.69							
Pixel-to-Pixel Flat-			0.20					0.20	
Field Stab. (<50 pix)				0.20					
Large-Scale Flat-					0.20				
Field Stab. (>50 pix)						0.20			
Inverse Sensitivity				0.52					
Function Stab.									
Telescope Trans-					0.30				
mission Stability						0.30			
NISP-P Through-							0.20		
put Stability								0.20	
Detector Stability									0.20
Spat. PSF Variation			0.30						
Stability									
Calibration Error in Pixel-to-Pixel FF (<50 pix)		0.20					0.17		Cal Plan
Calibration. Error in Large- Scale FF (>50 pix)		0.50							Cal Plan, MOCD
Detector Effect Correction Errors		0.73							
Bias and Dark Errors		0.29		Per Pixel:	1.00	1.00			NIRCam Value
Reference Pixel Correction Errors		0.29		Per Pixel:	1.00	1.00			NIRCam Value
Non-linearity Errors		0.30					0.20		NIRCam Value
Intrapixel Sensitivity Errors		0.40							Possibly smaller

Persistence	0.29	Per Pixel:	1.00	1.00	NIRCam Value
Electronic Ghosts and Cross Talk	0.29	Per Pixel:	1.00	1.00	NIRCam Value, to be discussed
Background Subtraction Errors	0.49			0.49	
Sky Subtraction Errors	0.35			0.35	NIRCam Value
Scattered Light Errors	0.35			0.35	NIRCam Value
Data Processing Errors	0.50				

Table 10: Relative photometric error budget allocations

6.2.8. R-WS.2.2-3

The NIR bands shall have an AB magnitude of 24 (in Y, J and H) for 5 sigma point sources.

Requirements on integration times given are based on this requirement through calculations in the Technical Note TN-00007_limiting_sensitivity_NISP_photometry_v4 (AD6).

To verify this requirement we compute limiting sensitivities and significance levels for a number of cases and in a number of ways:

- Two different PSFs (WA and WW from Section 5.1)
 - Two pixels scales (0.300 and 0.330 arcsec/pixel)
 - The three different photometric filter bands (Y, J, H)
- 1) We carried out a suite of simulations for the photometric mode and these parameters, using the requirement on telescope throughput, NISP PCE, backgrounds, integration times and detector properties. Below we evaluate these cases, in part with mean requirements assumed for the detector, but also with realistic detector maps as provided by TIS, scaled in the mean to the requirements for total detector noise, QE, and dark current. In these simulations a large number of point sources of 24 mag AB are distributed over a detector, and the images of three dithers are combined by drizzling to a final image, from which the sources are extracted via PSF fitting. The variation of extracted signal gives the noise of this process, and hence the S/N. In these simulations we leave out the 8% lowest weight objects in accordance with the lost-pixel requirement budget in Section 6.2.2.
 - 2) We evaluate the statistics of pixel-wise sensitivity for a given TIS detector by computing analytically the S/N for a single location, after combination of three dithers. This produces histograms of significance levels of detection for different object fluxes (evaluated from 23.5 to 24.0 mag AB). Here again the fluxes are extracted via PSF fitting.

- 3) The analytical calculation of limiting sensitivity is also done in AD6 (Technical Note TN-00007_limiting_sensitivity_NISP_photometry_v4). Here a 2x2 pixel aperture is used to extract the flux, with the other input parameters identical to the simulation input. It is actually these calculations that were used to define the current requirement on integration time.

The latter calculation was done before the current set of PSFs (Section 5.1) was defined and predictive assumptions were made about the actual width of the expected PSFs compares the PSF assumptions to the current WW PSF, expressed as the fraction of the point source flux ensquared in 2x2 pixels of 0.330"/pixel size.

Band	0.660" ESE assumed (P. Ferruit)	0.660" ESE current (WW PSF)	Conservative?
Y	0.68	0.641	✗
J	0.64	0.625	✗
H	0.55	0.598	✓

Table 11: Comparison of ensquared energies of PSFs assumed in integration time calculations and actual PSF

With the new PSFs available it turns out that in Y- and J-band the assumptions were still too optimistic, while too pessimistic in H-band. In addition and contrary to the full image simulations, the assumptions about the zodiacal light level in the Technical Note AD6 (TN-00007_limiting_sensitivity_NISP_photometry_v4, P.Ferruit) were lower than the average reference zodiacal light level. In combination, the TN calculations, which define the current integration times, did only partially account for the full effect of PSF broadening. Hence the PERD requirements on integration times computed in the TN calculations are too low and in return the actual limiting sensitivities, given all requirements including current integration times and PSF, will not meet the requirement level.

6.2.8.1. Limiting sensitivity requirement in the mean

We use the simulations and calculations in 1) and 2) above to quantify the extent of this, to define the impact on science and mitigation options.

Band	WA, 0.30"/pix Mean S/N	WA, 0.33"/pix Mean S/N	WW, 0.30"/pix Mean S/N	WW, 0.33"/pix Mean S/N
Y	5.72	5.79	4.25	4.41
J	5.99	6.03	4.42	4.56
H	6.54	6.56	4.95	5.08

Table 12: Mean S/N for 24 mag AB point sources in the nominal integration time

shows the mean significance of detections for the requirement 24 mag AB point sources. For the 3-dither case considered here, the “field average” (WA) PSF meets the S/N=5 requirement in the mean for all bands and considered pixel size cases, while the “field worst” (WW) PSF does not meet it for Y and J, and, depending on pixel size, marginally meets it in H-band.

6.2.8.2. Limiting sensitivity requirement distribution

If the requirement is considered to be not applicable in the mean, but for all objects, we can also compute the fraction of 24 mag AB objects or area for which S/N=5 is not reached. We have to remark that *the following is a major approximation* and made for purpose of discussing mitigation strategies only, since *it includes assumptions on how the actual PSFs widths will be distributed* over the FOV. For the sake of argument, we make the assumption that 70% of the area have the WA PSF (we assume >50% since some of the areas has a narrower PSF than WA and will offset part of the degrading effect of a somewhat wider PSF than WA, hence a combination of 3 dithers will average these), and 30% the WW PSF. Furthermore, 50.9% of the survey area will be covered by 4 dithers (Table 16), hence has substantially higher S/N. The fractions of objects for which S/N<5 both for the individual configurations, but also in the above scenario of mix of PSF distributions (last two columns) are shown in Table 13: These come on top of the 8% objects removed within the scope of the “lost pixel” requirement.

Band	S/N<5 WA, 0.30"/pix	S/N<5 WA, 0.33"/pix	S/N<5 WW, 0.30"/pix	S/N<5 WW, 0.33"/pix	Total S/N<5, 0.30"/pix	Total S/N<5, 0.33"/pix
Y (24AB)	23.4%	21.5%	77.3%	72.1%	19.4%	18.0%
J (24AB)	16.0%	15.1%	71.8%	66.9%	16.1%	15.0%
H (24AB)	6.1%	6.0%	51.8%	46.5%	9.7%	8.8%
Y (23.9AB)	11.1%	9.8%	63.7%	57.5%	13.2%	11.8%
J (23.9AB)	6.1%	5.8%	56.6%	50.3%	10.4%	9.4%
H (23.9AB)	1.8%	1.6%	33.8%	28.7%	5.6%	4.8%
Y (S*1.25)	<1%	<1%	29.2%	24.0%	4.3%	3.5%
J (S*1.25)	<1%	<1%	22.3%	18.1%	3.2%	2.7%
H (S*1.25)	<1%	<1%	7.1%	5.5%	1.0%	<1%

Table 13: Fraction of 24mag AB point sources with S/N<5 for different PSF and pixel scale cases in the 3 dither case. Given are the fractions for the different cases (columns 2-5) and the resulting total fractions under the assumptions of 50.9% of survey area covered with 4 dithers and 70% of FOV being covered by a WA and 30% by WW PSF. The bottom three rows show the same situation if through a mitigation process the signal is increased by ~25%, e.g. through longer integration times.

It is clear from the upper part of that in the current nominal case a non-negligible region of the FOV would not reach S/N=5 at 24mag AB, mainly through the effect of a wider PSF. This opens two areas for discussion, impact on science and mitigation options.

6.2.8.3. Science impact

WL is impacted through the dependence of photo-z error and catastrophic outlier fraction on S/N. The strength of the impact has been simulated (Hendrik Hildebrandt) and is shown in terms of the relative changes for a brighter limiting sensitivity compared to the 24mag AB

(point source, S/N=5) requirement. The relations that are shown are simulated for the case that in every photometric band entering the photo-z process a uniformly brighter limiting sensitivity is reached. If only one or some bands have different limiting sensitivities the overall change in outlier rate and error changes less than the depicted relation, however in a non-linear and hard to predict way, and differently for different galaxies and redshifts. The impact will also depend on the quality of the EXT ground-based data, since seeing variations will also lead to varying limiting sensitivities.

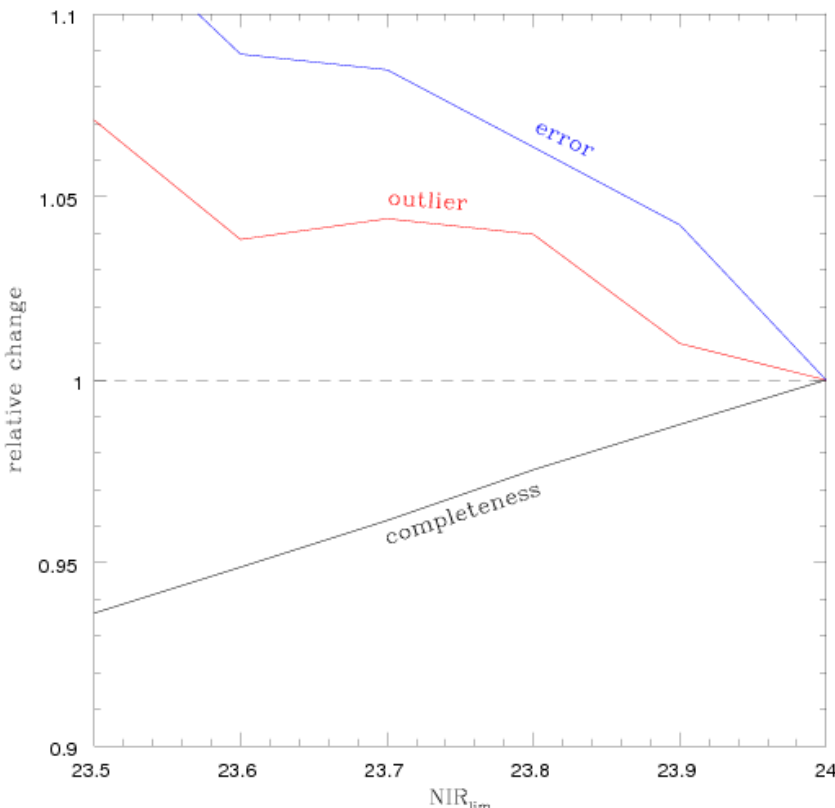


Figure 2, science impact: Relative change of photo-z outlier fraction, photo-z errors, and completeness from lower than required limiting sensitivity.

As can be seen from Figure 2, the relative change in error and outlier rate is rather small from limiting magnitude 24.0 to 23.9 (~1% higher outlier rate and 4% larger error; note, this is not an increase by 4% *points*), with larger steps from 23.9 to 23.8 and from 23.6 to lower values.

The current nominal mission parameters combined with the PSF-assumptions which entered mean that the 24mag requirement would be missed by ~20%/16%/10% of area or targets in the Y/J/H-band (first three rows in Table 13). Of these ~7%/6%/4% would lie in areas with 23.9-24.0mag limiting sensitivity, 9%/7%/5% between 23.7-23.9mag and 4%/3%/1% in areas worse than 23.7mag.

GC is impacted by a reduced completeness. We have taken the standard reference catalog by Roche/Zamorani of inferred target galaxy properties and computed the relative loss of galaxies with progressively brightening limiting sensitivity. The results are shown in Figure 3. The

relative completeness drops to 98.2% at 23.9mag, 96.3% at 23.8mag and 94.1% at 23.7mag limiting sensitivity.

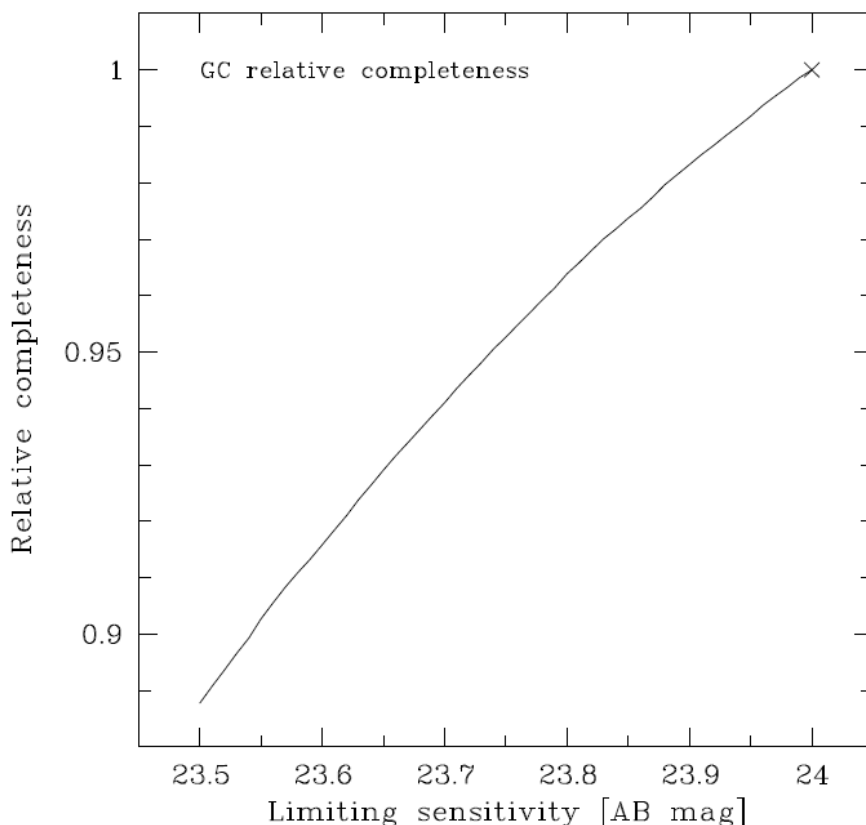


Figure 3: Galaxy clustering relative sample completeness as a function of limiting sensitivity, relative to the requirement value of 24mag AB, for the Roche/Zamorani input catalog.

If again the fractions of galaxies vs. limiting sensitivity are assumed (with 70% of area WA PSF, 30% WW PSF), then this corresponds to a total loss of ~1% of targets over the full FOV.

6.2.8.4. Mitigation options and tradeoff

Mitigating the impact on science can be done in three ways:

- 1) A search for hidden but unnecessary margins (“margins on margins”). The above calculation was done for a worst-case scenario, hence any hidden margin would make this approach overly conservative. At this point we identify one hidden margin, which lies in the requirement on the baseline Y-band filter curve, which implicitly set part of the NISP PCE requirements. While the requirement on the transmission was set to 74% across the filter band, the real-world filter curve that was used has a non-constant transmission but goes up to 86% at the red end, a first coating study by Zeiss confirmed this and showed that >90%

are technically not challenging. The increase in wavelength-weighted transmission is +13% or +21% in these two cases. There is no obvious margin of this scale for the other bands.

- 2) A stricter requirement on PSF width, aided by a more realistic sets of PSFs expectations on their spatial distribution.
- 3) An increase in exposure/integration time. An increase of the exposure times by 25% would lead to the recovery of required targets and a change in fraction of galaxies with S/N<5 at 24mag AB as shown in the last three rows of Table 13.

A combination of 1) and 3) could be used to re-balance limiting sensitivities to the same level. The exact required changes of exposure times are directly dependent on the assumptions on the PSF quality distributions. As an example: In again the case of above, an increase of exposure time by 25% in Y, 20% in J and 10% in H would roughly balance filters while pushing the fraction of galaxies with S/N<5 at 24mag below ~0.05. ~20% of this exposure time increase in Y could be absorbed by a changed filter requirement in 1). This would correspond to a total extra time needed of $4*(5s+19s+5s)=116s$ per pointing (or ~40 days extra integration time, while requiring no changes on dither/slew strategy or mechanism movements).

Overall, the limiting sensitivity requirement of 24 mag AB (point source, S/N=5)

- is met for the vast majority of galaxies/area for both WA and WW PSF in the 50.9% of the survey covered with 4 dithers
- is met for the 3-dither area and with the WA PSF in all bands in terms of mean limiting sensitivity (Table 12)
- is marginally met for the 3-dither area with the WW PSF in the H-band in terms of mean limiting sensitivity, but not in the Y- and J-band (Table 12)
- is hence not met for a non-negligible fraction of galaxies/area for all bands; actual fractions depend on the actual relative distribution of PSF widths.

Table 14 summarizes the current PERD requirements and an order-of-magnitude modification of this for compensating the effects of now wider PSF and higher than assumed backgrounds.

Photometry Band	Required Exposure Times	Exposure Time (with margins)
Y	100 s	~105 s
J	95 s	~114 s
H	60 s	~65 s
Total	255 s	~284 s

Table 14: The exposure times (excl. readout overhead) per dither required to meet the NISP Photometry Mode's 5σ detection limit. Exposure times for the nominal case and a TBC modification are presented.

While this modification still has to be discussed and final values to be calculated, these exposure times would lead to the limiting sensitivity requirement being met both in the mean, but (with

the explained assumption on PSF width distribution) also for all but a small fraction of the area, for which the science impact would be small.

6.2.9. R-WS.2.2-6

The survey shall be performed with 4 dithers in the visible and 4 dithers in each of the NIR imaging and spectroscopic channels.

Four small telescope dithers per pointing are planned in the survey design. The requirement is met.

6.2.10. R-WS.2.2-7

At least 95% of the survey shall be covered with 3 exposures in the visible bands and 90% covered by at least 3 exposures in each of the NIR imaging bands. Contiguous regions not covered by three or more exposures should have a size less than 5 arcmin².

Additional Text: For a galaxy to be useful for lensing it must have simultaneous imaging in both visible and the NIR.

There are gaps in the active coverage of the NISP focal plane. The three main contributors to dead area on the focal plane are:

- (i) Gaps between the detectors within the focal plane mosaic.
- (ii) The rows of reference pixels at the side of each detector. The baseline detectors (RD5) have 4 rows of reference pixels along each side, resulting in an active area of 2040×2040 pixels.
- (iii) The dead pixels within the detector active area. The dead pixels are not considered in the verification of this requirement; instead they are accounted for in requirement R-WL.2.1-13 (Section 6.2.2).

The four, small telescope dithers per pointing will, to some extent, fill these gaps between active detector areas. The baseline dither strategy is shown in Table 15 :

Pointing Number	Dither Pointing Shift
1	(0'', 0'')
2	(100'', 50'')
3	(100'', 0'')
4	(100'', 0'')

Table 15: The Euclid mission's baseline dithering strategy.

To validate this requirement we model the focal plane, accounting for the mosaic gaps and the reference pixels. The focal plane model is then shifted according to the dither strategy shown in Figure 4. We only consider the four dithers per field, we therefore make the worst case assumption that there are no overlaps between adjacent fields. The resulting sky coverage is shown in Figure 4.

The performance of this dithering strategy is summarized in Table 16.

Number of Dithers Imaged In	Fraction of Sky		Compliant
	Requirement	Performance	
> 4	(removed)	0.509	
> 3	> 0.90	0.934	✓

Table 16: Summary of the sky coverage assuming a dithering strategy of $(0'', 0'')$, $(100'', 50'')$, $(100'', 0'')$, $(100'', 0'')$.

This requirement is met.

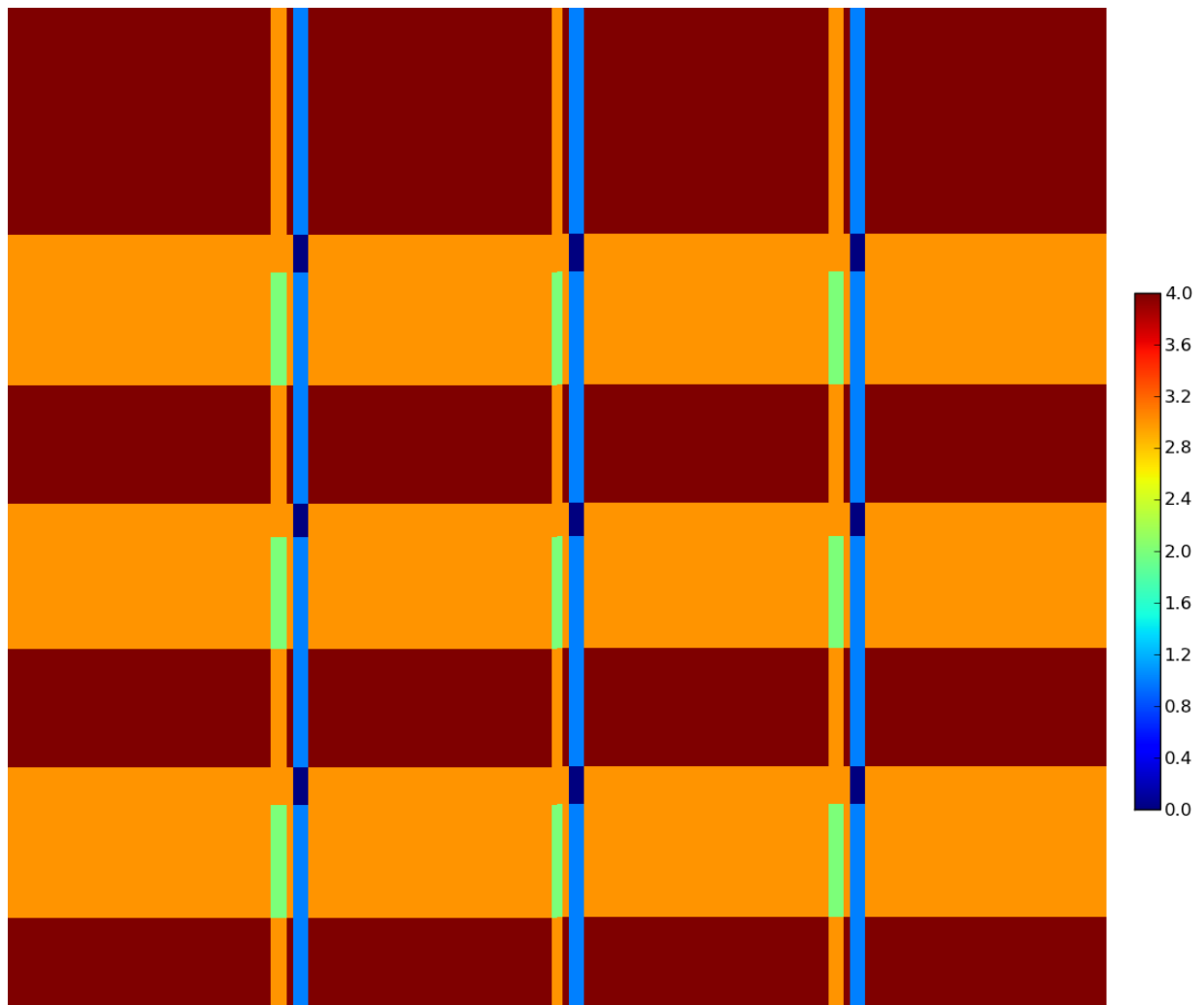


Figure 4: The sky coverage assuming a dithering strategy of $(0'', 0'')$, $(100'', 50'')$, $(100'', 0'')$, $(100'', 0'')$.

6.2.11. R-WS.2.2-10

NIR photometry of the fields covered by the slitless spectrograph shall be acquired, with depth fainter than AB=24 at 5 sigma (point source).

This requirement is identical to R-WS.2.2.3 and validated in Section 6.2.7.

6.2.12. R-DS.2.2-2

The depth of the stack of images shall be at least 2 mag deeper than the wide survey depth in both VIS and NIR

The deep survey is required to have the same depth per visit as the wide survey (R-DS.2.2-3, see Section 6.2.7). This requirement therefore translates into a requirement on the number of visits of the deep field.

To calculate the number of visits required to reach a detection limit of AB 26 mag (R-WS.2.2-3 + 2 mag), we assume that exposures are taken with the same mode as the wide survey are stacked. We assume that the individual exposure times are the same as those calculated in Section 6.2.7.

The 5σ detection limit of the photometry mode of the NISP instrument as a function of the number of deep field visits is shown in Figure 5.

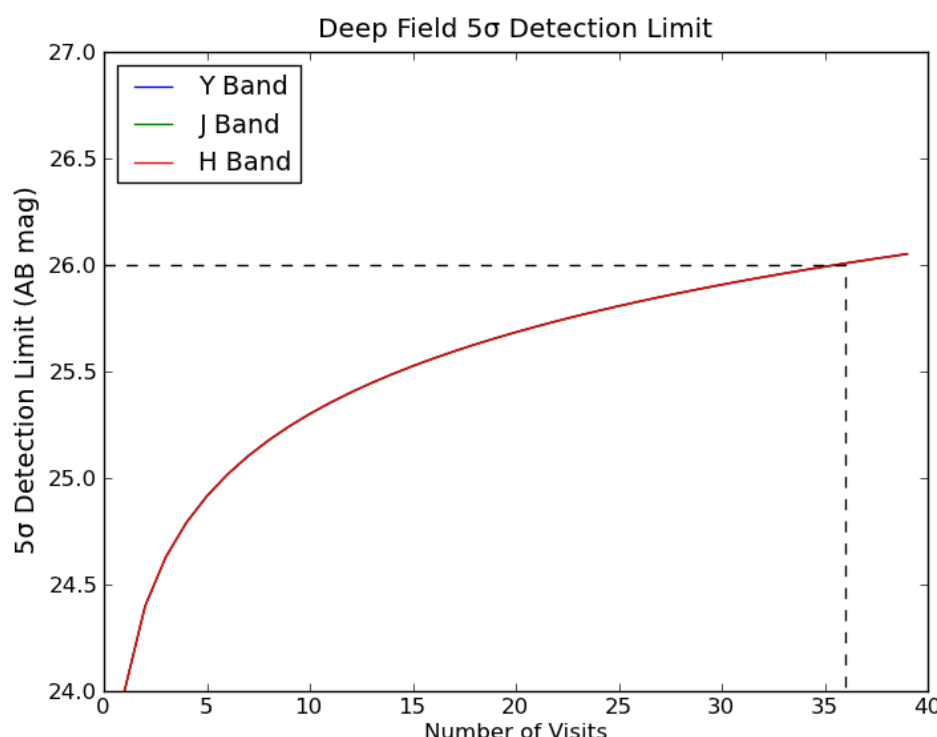


Figure 5: The 5σ detection limit in the deep field as a function of the number of visits. The observing mode in each visit is the same as for the wide survey.

The number of deep field visits requirement to meet the 5σ detection limit is presented in Table 17.

Depth Requirement	Number of Visits to Deep Field		Compliant
	Requirement	Allocated (AD5)	
26 AB 5σ	> 36	40	✓

Table 17: A summary of the number of visits to the deep required to meet the 5σ detection limit.

This requirement is met.

6.2.13. R-DS.2.2-3

Depth per visit: same as for the wide survey

The deep fields will be observed with the same observation mode as the wide survey (R-DS.2.2-13, AD2). This requirement is therefore identical R-WS.2.2-3 and R-WS.2.2-10.

7. Spectroscopy

In this part, the performance of the spectroscopic channel is evaluated. This covers the instrumental configuration, the verification of Level 2 requirements and of a large part of Level 1 requirements.

First we will summarize the requirements, which have been flow down from AD1 through AD2 to AD3 and AD4, and the values used in simulation.

Then we will summarize the performance evaluation scenarios and the assumptions we have made on some parameters. Finally verification results and performance will be presented.

We will define requirements for

Performance (section 7.1): These are the requirements from AD1 which for verification require implementation of instrument parameters and observational strategy as from AD2 to be verified.

Instrument (section 7.2): These are the requirements, which have been flown down in AD3 through AD2. They refer to AD3 and are used as inputs to the simulations.

Survey (section 7.3): refers to requirements, which are defined for the wide survey in AD1, flown down in AD5 and are implemented in the observational strategy.

Verification and simulation of the full survey, as well as of the sky coverage is not part of this work, and is addressed in another document.

7.1. Applicable requirements

Table 18 summarizes the Level 2 requirements for spectroscopy applicable for the performance evaluation. Indicated in the last column, the level of verification. . The last column indicates the level of verification attained.

Reference	Description	Requirement	implementation	Compliant
GC.2.1-1	Flux limit	$< 3 \times 10^{-6} \text{ erg cm}^{-2} \text{ s}^{-1}$	Performance	✓
GC.2.1-2	Completeness	$> 45\%$	Performance	✓
GC.2.1-3	Variation in Flux limit vs. wavelength	$< 20\%$	Performance Calibration	✓
GC-2.1-10	Calibration subsample	140000 gal , purity $> 99\%$	Deep survey	✓

Table 18: Level 2 requirements for performance verification in spectroscopy

7.2. Instrumental configuration overview

Table 19 summarizes the instrument configuration and parameters, which will be described in the next sections and have been derived from AD1.

The requirements have been set to be the ‘worse case’ scenario.

Anyway sensitivity analysis around the main parameters, mainly PSF and detector performances, will be presented in section 7.11.2 to estimate margin and possible degradations.

reference	Instrument Parameter	Value	Parent (AD1)
R-NIS-P-008	FOV	0,54 deg ²	R-WS.2.2-1
	Plate scale	0,3+=0,03'' by px	
R-NIS-F-012	Grism bands (nm)	Blue=1100-1457 Red=1445-2000	GC.2.1-4
R-NIS-P-002	Out of band	10-3	GC.2.1-1
R-NIS-P-003	Dispersion/pixel	9.8A/pix	GC.2.1-5
R-NIS-P-001	transmission	See curve in section 7.5	GC.2.1-1
R-NISP-P-002	Optical PSF EE in radius (asec) average	Double Gaussian Blue EE50= 0,18'' EE80 = 0,45'' RedEE50=0,22'' EE80 = 0,57''	GC.2.1-1 GC.2.1-2
	Detector PSF	4 nm	GC.2.1-1
R-NIS-P-002	Noise (instrument entrance)	Blue = 1 e s ⁻¹ pix ⁻¹ Red = 0,99 e s ⁻¹ pix ⁻¹	GC.2.1-1
R-NIS-P-007	Instrument noise	Blue<0,093 e s ⁻¹ pix ⁻¹ Red <0,093 e s ⁻¹ pix ⁻¹	GC.2.1-1
R-6232-8	Scatter light noise	Blue <0,1 e s ⁻¹ pix ⁻¹ Red < 0,1 e s ⁻¹ pix ⁻¹	GC.2.1-1
R-NIS-F-009	Integration time	565s	GC.2.1-1

Table 19: instrument parameters for performance evaluation

Comment on exposure/integration time:

The time given in AD3 is the integration time including the frame reading time. In spectroscopy, we allow 5 s for the detector frame read and 560 s of effective exposure time available for science. **In the following evaluation, we will use only the scientific exposure time of 560s.**

7.3. Observational strategy overview

The reference (AD3 or AD4) and parent requirements from AD1 for the wide survey are listed Table 20.

Reference	Description	Requirement	Parent
R-NISP-I-004	Wide Survey field overlap	minimum	WS.2.2-5
R-520-4	Dithering I	≥ 4 NIR channels	WS.2.2-6
R-520-4	Dithering II	90% with ≥ 3 NIR channels	WS.2.2-7
R-NIS-F-002	Wide Survey NIR spectroscopic dithering	Different orientation/filters	WS.2.2-8
R-INS-F-002	NIR image for spectroscopy	AB=24	WS.2.2-10
R-NIS-F-009	NIR integration time	Sufficient to reach flux limit	WS.2.2-11

Table 20: wide survey parameters for spectroscopy

The observational strategy derived from these requirements is then based on 4 dither frames:

- 2 dithers with a rotation of 90 degrees in the blue band
- 2 dithers with a rotation of 90 degrees in the red band

7.4. Optical parameters description and justification

7.4.1. Spectral bands

- The blue grism covers from 1.1 to 1.457 micron
- The red grism covers from 1.445 to 2 micron

7.4.2. PSF evaluation

The PSF values have been agreed with ESA through requirements on EE80 and EE50 values. In Table 21, EE values corresponding to 3 different assumptions of PSF values across the field are summarized.

Case 1: worst ESA Case

	Y	J	H	B	R
EE90 in arcsec	1,06	1,06	1,24	1,1	1,26
EE80 in arcsec	0,53	0,53	0,62	0,55	0,63
EE50 in arcsec	0,29	0,3	0,31	0,3	0,32

Case 2: Mean ESA Case

	Y	J	H	B	R
EE90 in arcsec	0,76	0,86	1,14	0,9	1,14
EE80 in arcsec	0,38	0,43	0,57	0,45	0,57
EE50 in arcsec	0,18	0,18	0,2	0,18	0,22

Case 3: Worst ESA Case + 10%

	Y	J	H	B	R
EE90 in arcsec	1,17	1,17	1,36	1,21	1,39
EE80 in arcsec	0,58	0,58	0,68	0,61	0,69
EE50 in arcsec	0,32	0,33	0,34	0,33	0,35

Table 21: EEs values agree with ESA for average, worst cases for performance evaluation

The final values for the PSF, used in simulation, are then computed from a double Gaussian fit of the optical median value and the encircled energy value is:

The presented document is Proprietary information of the Euclid Consortium.

This document shall be used and disclosed by the receiving Party and its related entities (e.g. contractors and subcontractors) only for the purposes of fulfilling the receiving Party's responsibilities under the Euclid Project and that the identified and marked technical data shall not be disclosed or retransferred to any other entity without prior written permission of the document preparer.

$$EE(x) = \frac{C\sigma_1^2(1 - e^{\frac{-x^2}{2\sigma_1^2}}) + (1 - C)\sigma_2^2(1 - e^{\frac{-x^2}{2\sigma_2^2}})}{C\sigma_1^2 + (1 - C)\sigma_2^2}$$

The parameters are:

C is the amplitude of the first Gaussian
 σ_1^2 is the variance of the first Gaussian
 σ_2^2 is the variance of the second Gaussian
 r^2 is the radius $r^2=x^2+y^2$

The values for each spectroscopic bands are summarized in Table 22 is added quadratically.

PSF contribution	Blue	Red band
c	0.98861	0.989358
σ_1	0.123389	0.150535
σ_2	0.664314	0.840262
EE50 radius (arcsec)	0,18	0,22
EE80 radius (arcsec)	0,45	0,57
FWHM (arcsec)	0,4	0,49

Table 22: Parameters for the PSF evaluation in the average case (WA)

PSF contribution	Blue	Red band
c	0.987238	0.989894
σ_1	0.218437	0.226849
σ_2	0.94468	0.989831
EE50 radius (arcsec)	0,3	0,32
EE80 radius (arcsec)	0,55	0,63
FWHM (arcsec)	0,67	0,71

Table 23: Parameters for the PSF evaluation in the worst case (WW)

The FWHM is estimated by its relation with EE50 which, for a single Gaussian is EE50 (radius)~0,45 FWHM. As the second Gaussian contributes by only 2%, and only in the outmost part of the function, this is an acceptable approximation.

Evolution of the PSF with the wavelength

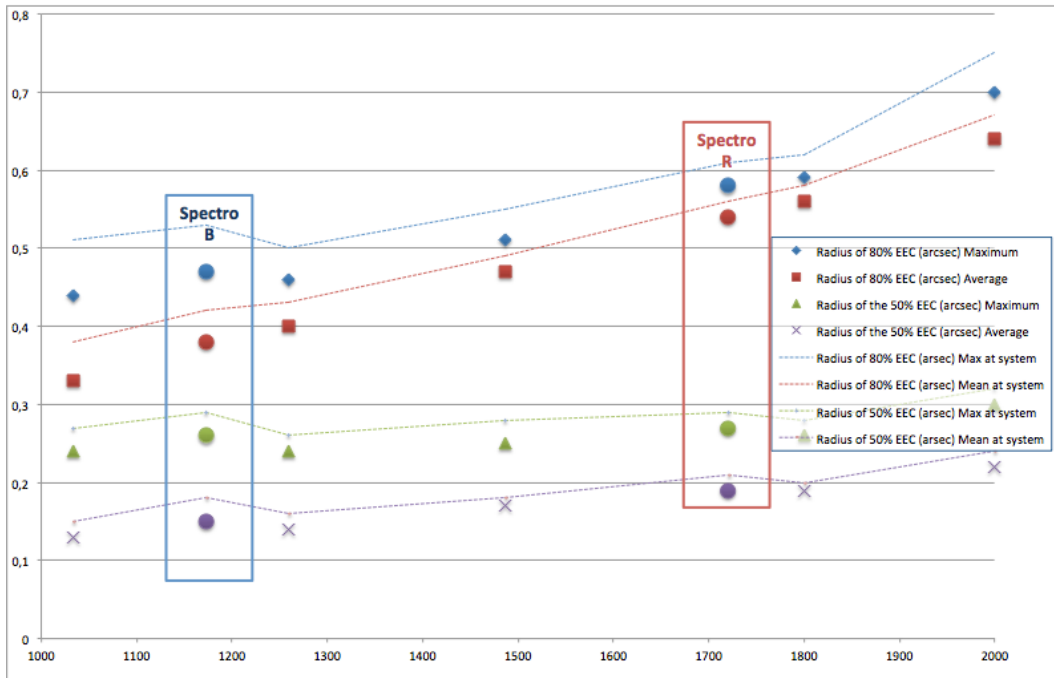


Figure 6: the evolution of the PSF in function of the wavelength

As we see on figure 7, due to diffraction effect, the PSF has a significant slope in EE80 and a smaller one in EE50. This should be evaluated and we consider a linear evolution so that at 2 micron the encircled energies in the red are EE50=0,35'' EE80=0,75''. We will do some evaluation of the implication of this slope mainly in the red (called WR afterwards).

7.4.3. Resolution element evaluation

The resolution per pixel is estimated from the EE50 values and the requirement GC.2.1.5 applied to a 1'' object diameter. The convolution for the average and worst EE50 gives the number of pixel (FWHM/0,3''). The required resolution is $R > 250$ for $\lambda \geq 1.1$ micron (GC.2.1.5). This translates in a dispersion by pixel by:

$$R = 250 > \lambda / (\text{npixel} * \delta\lambda)$$

	Red average	Red worst
FWHM	0,49	0,71
npixel	3,7	4,1
$\delta\lambda$	9,8	11,1

Table 24: dispersion per pixel for the 2 PSF (average and worst) cases considered in this study

On the other hand we don't want to have too long spectra in the larger band (the red one) . Accepting spectra with a maximum length of 600 pixels from 1.44 to 2 mm, we get 560 nm/600 pix= 9,3 nm/pixel.

Thus the dispersion per pixel should be in the range

$$0,93 \leq \delta\lambda < \leq 9,8 \text{ \AA}$$

The current value for the dispersion is 9,8 \AA and is compliant with the requirement.

7.5. Instrument throughput evaluation

7.5.1. Instrument transmission

7.5.2. Telescope

The value reported in Table 25 are from RD4 and should be taken for lambda > 1 micron to 2 micron. They include both telescope and dichroic (see also Figure 7)

Wavelength (in microns)	0.92	0.95	1.00	1.10	1.30	1.50	1.70	2.00	2.10
Minimum transmission	0.276	0.567	0.773	0.773	0.773	0.773	0.773	0.773	0.773

Table 25: telescope throughput

7.5.3. Optical transmission

The optical transmission of the instrument includes the following elements

- Collimator
- Grating
- Filter
- Camera

The evaluation reported in this report is done for the worst case scenario for the optical instrument throughput (without the detector) . As seen in Figure 7, the blue throughput of the instrument has been taken flat at 0,385 and the red values are from a straight line starting at 0,55 at the 1,45 micron down to 0,32 at 2 micron. These values are given as requirements in RD3.

7.5.4. Detector quantum efficiency

For this evaluation, the QE of the HdCdTe detector is taken as 70% flat on all the range and is an EOL value (AD5). The current specification is of 75% BOL. It has been specified to the vendor that the radiation test damage should not degrade the QE by more than 5 %. This should ensure the 70 % EOL.

The current specification of 75 % has been agreed to be a mean value on the detector pixels and not a worst value. This mean value is only for ‘operable pixels’ (for definition and discussion on operable pixels see section 7.7.1)

It is not possible in this report to give the assumption of RMS as it is TAA information or even to specify this RMS. It should anyway be noticed that this information has been given by the vendor for some representative devices, allowing to do performance test that will be reported in section 9.

7.5.5. Contamination and out of band transmission

The out of band transmission for the blue and red band is taken to be 0,1 % % (RD3).

The out band transmission is meant to remove contribution from other wavelengths (zodiacal, thermal contribution) in the blue and red band. It is particularly important at 2 micron as we now use a 2.4-micron cut off detector, and on the blue edge, as we want to reduce the noise and then to use a reduced band compared to the photometric channel.

7.5.6. Total transmission

Figure 7 summarizes the different values reported in 7.5.3, 7.5.4. To satisfy GC.2.13, it is required that the total transmission should not vary more than 20% between the blue and red. The current values satisfy this requirement. For completeness, we indicate the value used in previous evaluation as ‘red book’ as they can be considered as ‘nominal values’ for the instrument.

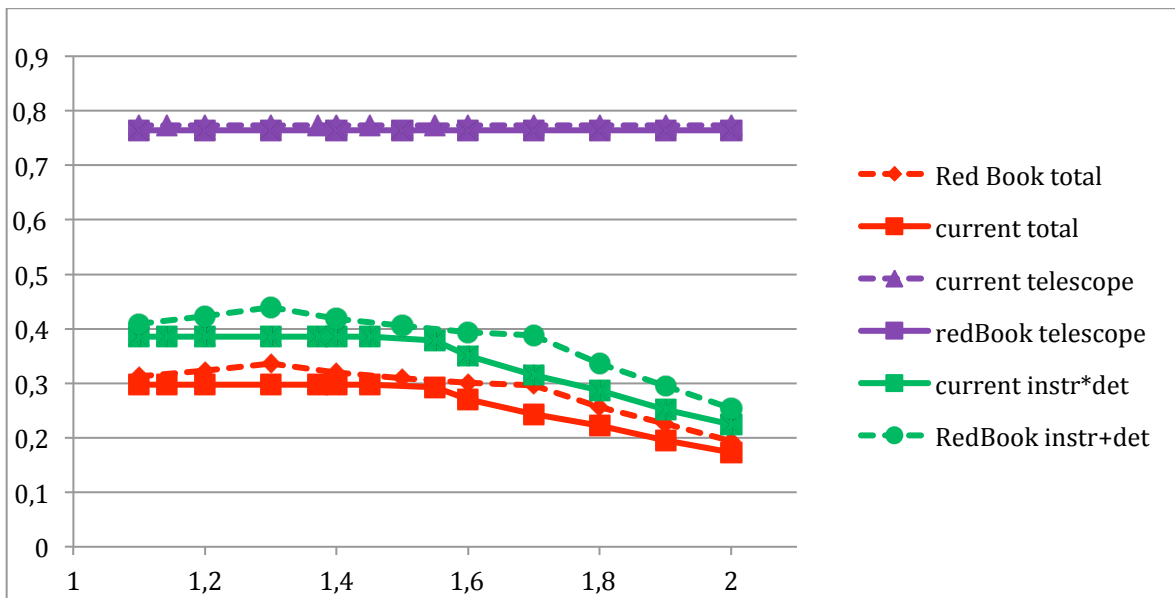


Figure 7: Transmission for the spectroscopic channel

7.6. Radiometric evaluation

7.6.1. Zodiacal noise

In a slitless configuration, the noise coming from the sky, after passing through the telescope is integrated in the full grating band. To calculate the sky noise we should evaluate the integration of the value from 1.1 to 1,475 μm in the blue band, and from 1.445 to 2 μm in the red band. In both cases the entrance flux is reduced by the telescope transmission given in 7.5.6. These values have been calculated and nominal values are given as requirement. They are at the level of 1 e/s/pixel at the instrument entrance (AD3). We should mention than this nominal value can vary in the survey and can change field to field. We will examine in this report in section 8 and 10, the effect of such variation on final performance.

7.6.2. Detector noise

The current requirement is a total noise <9.5 e RMS (EOL). This value allow to not been detector noise limited as it can be seen from RD6. To be able to reach such a level of noise, a continuous up the ramp will be implemented (RD4). W should mention also here

- the BOL value has been specified to be 9e and the degradation due to radiation should not exceed 5% , leaded to the EOL of 9.5e.
- this value is a total noise mean value on the detector pixels and not the worst value

The specification is also given on the total noise which include

- the dark noise contribution
- the final read noise avec the continuous up the ramp procedure.

7.6.2.1.1. Dark current

The current implementation baseline is a 2.4 micron cut off HgCdTe detector at a temperature of 100 K. The expected dark current is <0,1 e/s/pixel.

7.6.3. Other noise contributions

Other contribution are (see AD3) for requirements:

- the telescope scatter light at the entrance of the instrument with an allocation of 10% of the zodiacal noise (0,1 e/s/pixel)
- the instrument noise on the detector plan, with another 10% of the zodiacal light (< 0,093 e/s/pixel). In this case, such 10% should take into account thermal contribution, scattered light and whatever other looses.

The 10% allocated to the telescope is sensitive to the full optical path and thus should be multiplied by the global transmission given in section 7.5.6. The final values have been computed in RD2 and are given in RD3. The instrument part is assumed not to pass through the

optics and thus is directly accounted for the detector and affected only by the quantum efficiency.

A precise evaluation of this contribution would require a sophisticated scattered light model, which has not been developed yet. The thermal noise of the instrument has been evaluated in the instrument radiometric evaluation and shows that this part will remain inside the specification (see RD6). The stronger contribution will be on the red band, coming from the telescope. The *diffuse* scattered light from the instrument optics and surrounding structure is expected to be very small but it is too early to have a complete model. A more precise estimation will be done in the next phase.

7.7. Other parameters

In this section, parameters needed for performance evaluation are recalled.

7.7.1. Number of operable pixels

The detection is done on 16 arrays of 2040x2040 operable pixels (AD3)

The current operability is of 95% BOL (AD5). The operability criteria has been worked out with the vendor and in the current study we call non operable pixel a pixel which has :

- a QE lower than 30% than the requirement (for 75 % , it is $\text{QE} > 45\%$)
- a total noise more than 18 e (2xthe specified value)

The impact on the science results is presented in 7.11.4

7.7.2. Pixel response variation in one detector

The variation of the performance pixel to pixel in one detector should be studied in detail as the final distribution of each parameter will impact the science result.

We have received some realistic information form the vendor and this make us able to test the impact of the QE and noise distribution on the science image (mean, rms and tail). Some results will be shown in 7.11.2. but as these distributions are under TAA restriction, we will not shown them in this report and we will only give results of their effect.

7.7.3. Pixel size and plate scale

The plate scale has been fixed to be $0.3'' \pm 0.03''$ on 18 ± 1 micron . The impact of the size is evaluated in section 7.11.4

7.7.4. Gaps between detector

The current detector implementation has gaps in X of 3 mm and gaps in Y of 6 mm (AD3 and RD8)

7.8. Observation parameters

7.8.1. Exposure time

The value taken in the presented evaluation is of 560 s for one exposure in agreement with the global survey strategy. The total integration time is of 565s. This allow to take into account the time for the up the ramp (if we don't use the first or last frames: we recall than the time between individual frame is 1,3 s).

Observational scenario:

The current implementation is based on 4 frames dithered as in 7.8.2
 The baseline configuration and observation mode is defined as

- 2 frames of 560s exposure (565 s integration) in the blue band rotated by 90 degrees each (position 1 and 2 of the GWA Wheel)
- 2 frames of 560s exposure in the red band rotated by 90 degrees each (position 3 and 4 of the GWA Wheel)

The 4 frames are dithered with the strategy described in section 0 to be able to fill detector gaps. This observational strategy has been shown to be the one which best allows to account for object to object spectral contamination, allowing to reach requirement GC.2.2.2

7.8.2. Dithering strategy

See Section 6.2.10

7.8.3. Cosmic rays

The cosmic ray rate is estimated to affect between 5% to 20% of pixel in one exposure of 560s depending of the shielding option.

Cosmic rays can also be reduced by implementing a rejection algorithm thanks to the detector readout mode, based on an up the ramp procedure. The implementation on processing to have this kind of rejection has been studied and is currently foreseen (RD3).

For the few cosmics which would escape the up the ramp based rejection, detection and rejection on the 2D spectra may also be possible later on ground.

As a rejection solution seems reliable in all cases, this explain than current performance evaluation ignore their effects. We expect only degradation in the signal to noise of the affected pixel by a factor less than 1.4. The impact of this degradation on a line extraction with a realistic distribution will be studied in detail in the next phase.

7.9. Summary of parameters used for performance evaluation

Table 26 reports the list of parameters used for performance evaluation. We emphasize that these parameters should be taken as EOL values. The breakdown will be treated at the sub system level in the instrument.

Reference (AD3 /AD4)	Instrument Parameter	Value	Parent (AD1)
Instrument parameters			
R-NIS-P-008	FOV	0,54 deg ²	R-WS.2.2-1
	Plate scale	0,3+=0,03'' by px	
R-NIS-F-012	Grism bands (nm)	Blue=1100-1457 Red=1445-2000	GC.2.1-4
R-NIS-P-002	Out of band	10-3	GC.2.1-1
R-NIS-P-003	Dispersion/pixel	9.8A/pix	GC.2.1-5
R-NIS-P-001	transmission	See curve in section 7.5	GC.2.1-1
R-NISP-P-002	Optical PSF EE in radius (arsec) average	mean/worst Blue EE50= 0,18'' /0.3'' EE80 =0,45''/0,55'' Red EE50=0,22''/0,32'' EE80=0,57''/0,63''	GC.2.1-1 GC.2.1-2
	Detector PSF	4 nm	GC.2.1-1
R-NIS-P-002	Noise(instrument entrance)	Blue = 1 e s ⁻¹ pix ⁻¹ Red = 0,99 e s ⁻¹ pix ⁻¹	GC.2.1-1
R-NIS-P-007	Instrument noise	Blue<0,093 e s ⁻¹ pix ⁻¹ Red <0,093 e s ⁻¹ pix ⁻¹	GC.2.1-1
R-6232-8	Scatter light noise	Blue <0,1 e s ⁻¹ pix ⁻¹ Red < 0,1 e s ⁻¹ pix ⁻¹	GC.2.1-1
R-NIS-F-009	Integration time	565s	GC.2.1-1
Survey parameters			
R-NISP-I-004	Wide Survey field overlap	minimum	WS.2.2-5
R-520-4	Dithering I	\geq 4 NIR channels	WS.2.2-6
R-520-4	Dithering II	90% with \geq 3 NIR channels	WS.2.2-7
R-NIS-F-002	Wide Survey NIR	Different	WS.2.2-8

	spectroscopic dithering	orientation/filters	
R-INS-F-002	NIR image for spectroscopy	AB=24	WS.2.2-10
R-NIS-F-009	NIR integration time	Sufficient to reach flux limit	WS.2.2-11
Detector parameters			
R-NISP-I-004	Number of Detectors	4×4	
R-NIS-P-013	Pixel size (arcsec)	$0,3'' \pm 0,03''$	AD2
R-NISP-I-005	Gaps between Detectors	$3 \times 6 \text{ mm}$	AD2
	Quantum Efficiency	0.7	RD5
R-NIS-P-009	Total noise in 560 s	9.5 e-	AD2
	Detector PSF	Gaussian, FWHM = 4 μm	AD2
	Detector Cut-off	2.4 μm	AD5

Table 26: Summary of spectroscopic instrument parameters used in simulation

7.10. Flux limit evaluation (GC.2.1-1 and GC.2.1.3)

7.10.1. Method

To verify the line sensitivity and evaluate its margin versus wavelength and parameters, an ETC (exposure time calculator) has been used. There are currently two different and independent implementations available: the first one is directly connected to the End to End Simulations described in 7.11, and is the one used in the AO for previous estimations. The second one under direct control of the Instrument Scientist has been developed for faster evaluation and is currently used for all radiometric and sensitivity evaluations. A direct comparison of the 2 tools has been done on different SNR values and has shown to be in perfect agreement as it is reported in 7.10.2.2

The ETC is implemented with standard signal to noise formulae which takes into account describes with the following terms;

$$\text{SNR} = S / \sqrt{S + N_{\text{pix}} * (B + D)}$$

- S is the signal on pixel coming for the line. The evaluation of the signal is computed as:

$$S = F(\lambda) * A(\lambda) * \epsilon(\lambda) * QE * t_{\text{exp}} * s(\lambda)$$

Where

-**F(λ)** is the initial flux in $\gamma/\text{cm}^2/\text{s}$

-**A(λ)** is the effective area of the OTE

- **$\epsilon(\lambda)$** is the transmission (included OTE) . The different efficiencies are the one described in section 6.5.2.

-**QE** is the quantum efficiency of the detector

-**texp** is the time exposure which can be divide in multi frame. IN this case we can write

$$\text{Nexp} = \text{texp} / \text{tframe}$$

In the current implementation, Nexp=2 and tframe = 560s

-**s(λ)** is the signal used in the estimation and depends of the extraction, For the extraction of narrow emission line, we are not sensitive strongly to pixel to pixel variation as for a continuum but mainly to the extend of the PSF. It is why in this evaluation; we will mainly used 80% of the total flux.

- **Npix** represents the number of pixel on which the line is extracted. The number of pixel depends of the image quality and of the PSF. The evaluation of Npix is difficult for an extended source as the object size will spread also the signal in many pixel and we should convoluted the 2 effects. Then, to extract the line, the result will depend strongly on the way we can do the extraction in the future and on the possible weighting of pixel that we can expect from an optimal extraction. It is difficult to evaluate correctly this number. Then we have implemented a conservative approach based on EE80 and have made an evaluation of the margin expected the final result (see section 7.10.2.5)
- **B** represents the noise introduced by the different noise contribution (no detector) as described in section 7.6.1. For this evaluation we assume this contribution to be the zodiacal light plus a noise corresponding to 20% of this value. To take into account the current breakdown of noise we assume that:
 - 10 % of the zodiacal contribution is added passing all the optical path (mean is affected by the total transmission)
 - 10% of this contribution is coming from the instrument and is not affected by the optical transmission but only by the QE of the detector.
- **D** represents the total noise coming from the detector. It is composed of the dark contribution and of the readout noise contribution and is by pixel calculated by

$$\text{Var(D)} = \text{sqrt}(D) = \text{sqrt}(DC * \text{texp} + nexp * R^2)$$

Where DC is the dark current value in e/s/pixel and R is the readout noise in e RMS. This parameter is one of the most critical for determining the sensitivity and will be evaluated in detail in section 7.10.2.3

The reference flux $F(\lambda)$ used in this evaluation is of 3×10^{-16} erg/cm²/s for an 1'' diameter size object. The sensitivity is of 3.5σ at a wavelength of 1.6 micron as required in GC.2.2.1.

To compute the flux limit, the SNR is computed using an exposure time of 2x540s otherwise specified, in agreement with the observational scenario described in section 0 and on the blue and red band simultaneously. We also verify to not have a variation of more than 20 % of this detection on the full band from GC.2.2.3

Unless otherwise specified, the blue band results presented in this document refer to computations performed at the reference wavelength of 1.2 μm, while red band results are obtained at the reference wavelength of 1.7 μm.

7.10.2. Results

In this section we have explored the effect of different parameters entering in the sensitivity evaluation. We use previous parameters as EOL to be able to estimate the reference performance. We have also studied some parameters in more details to evaluate their impact on the performance and possible margins. In particular we have evaluated:

- The optical image quality which is directly related to the number of effective pixel used for the line extraction (section 7.10.2.5).
- The noise estimation in particular if thermal contribution is compliant with the current requirement (GC.2.2.11)
- The detector parameters (QE and noise) in section 7.10.2.3

The final performance evaluation is based on the verification that we can reach the expected flux limit required in GC.2.1 with the EOL worst parameters on all wavelengths.

7.10.2.1. Image quality and number of effective pixels

In the evaluation, the number of effective pixel is calculated as the convolution of an uniform circular galaxy with EE80 taken as also as a box.

This gives an equivalent area of 25 pixels (5x5) under the line for a 1'' object size and an EE80 of 0,6''. This is a very conservative value as we can estimate that a better extraction will be possible using 16 pixels under the line. Also, a realistic number of pixel will depend of the object size. Figure 8 show the evolution of the number of pixel for the EE80 value and the object size. The object size is in average around 0,6'' in diameter . The 1'', as defined in the requirement , can be considered as a 'worst' case for sensitivity estimation as it implies to take the larger number of pixel under the signal.

We have estimated the effect of this number of pixel and this is presented in the flux limit result.

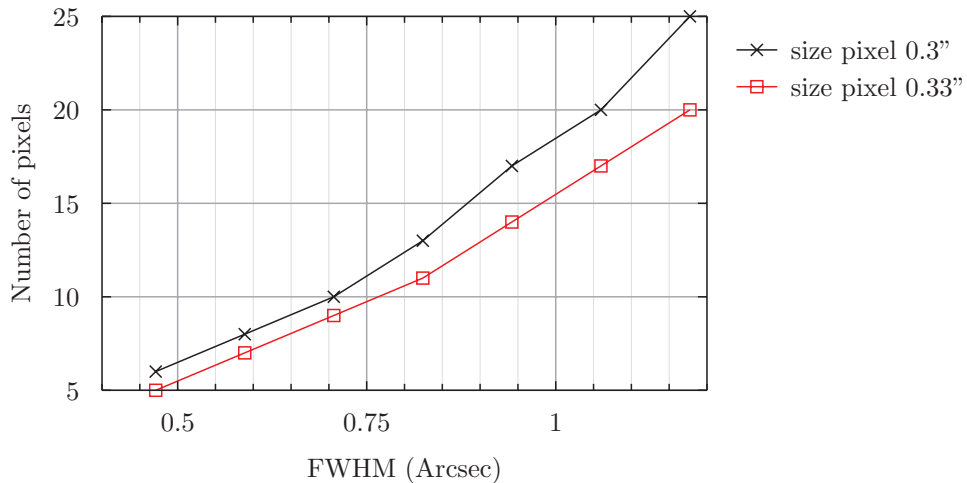


Figure 8: the number of pixel under the emission line in function of the object size convoluted with the PSF FWHM.

7.10.2.2. SNR versus line flux

We first verify the compliance of the signal to noise for 2x560s, other parameters fixed as described in Table 26, at two different wavelengths (1.1 micron and 1.6 micron), and in function of the line flux and of the exposure time. The requirement is to reach an SNR of 3,5 s in the 2 bands for a flux of 3×10^{-16} erg/cm/s. In Figure 9, we see that the required S/N is reached easily in the red band. The blue band is more dominated by the zodiacal noise and has poorer performance but it is still compliant with the requirement.

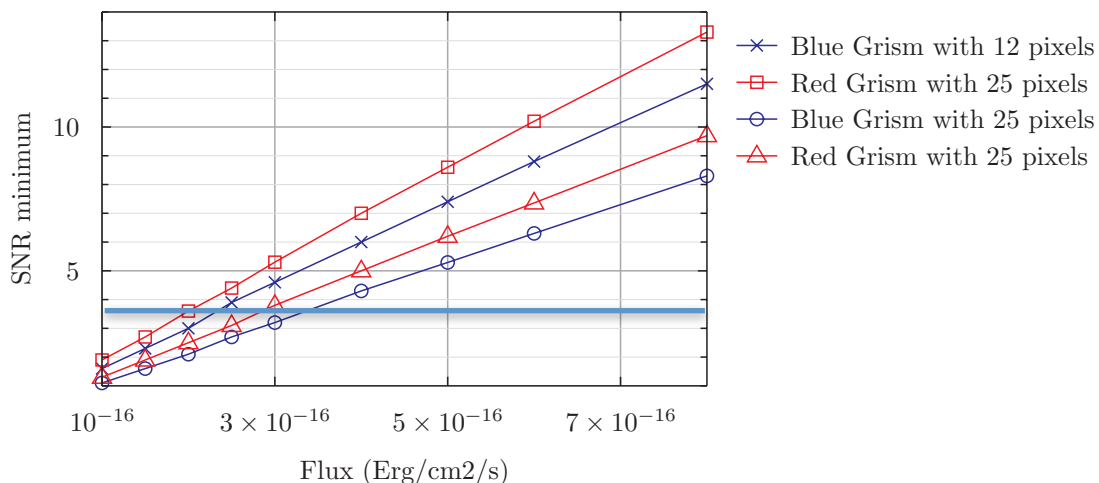


Figure 9: Signal to noise function of the flux on the line for 2x560s exposure time for 2 assumption of the number of pixel under the emission line. the requirement (blue line) is to have SNR>3.5 sigma at 3 10-16 erg/cm2/s

We represent also on

Figure 10, the signal to noise in function of the exposure time of one frame on a 1'' object, for 2 assumptions of number of pixels under the line (5x5 and 12 pixel which is what we should expect with the current average PSF).We see than the current exposure time allows reaching the requirement in flux in the 2 bands but we are at the limit in the blue band if we consider 25 pixels.

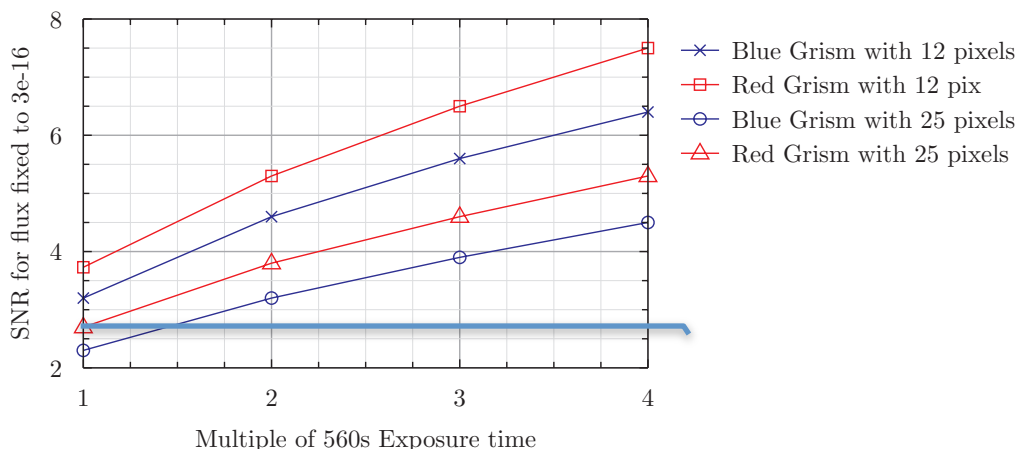


Figure 10: Signal to noise versus the exposure time. We see that we are just at the requirement for the blue band for 25 pixels and 2 exposures of 560s. There is clearly more margin in the red band.

7.10.2.3. Estimation and validation of the detector parameters for the current configuration

To verify and estimate the sensitivity to detector parameters, we have separated the detector contribution from the other parameters of Table 26 and have plotted on Figure 11 the total detector noise (dark and readout) in 560s as a function of the QE of the detector, keeping other transmissions values fixed at the EOL evaluation. If we fixe QE of 70 % for the detector, there is a strong constraint on the total noise which should be reduced to 9 e⁻. 9e⁻ can be declined as 7 eRMS readout and 0,05 e/s/pixel but can be differently distributed depending of the detector.

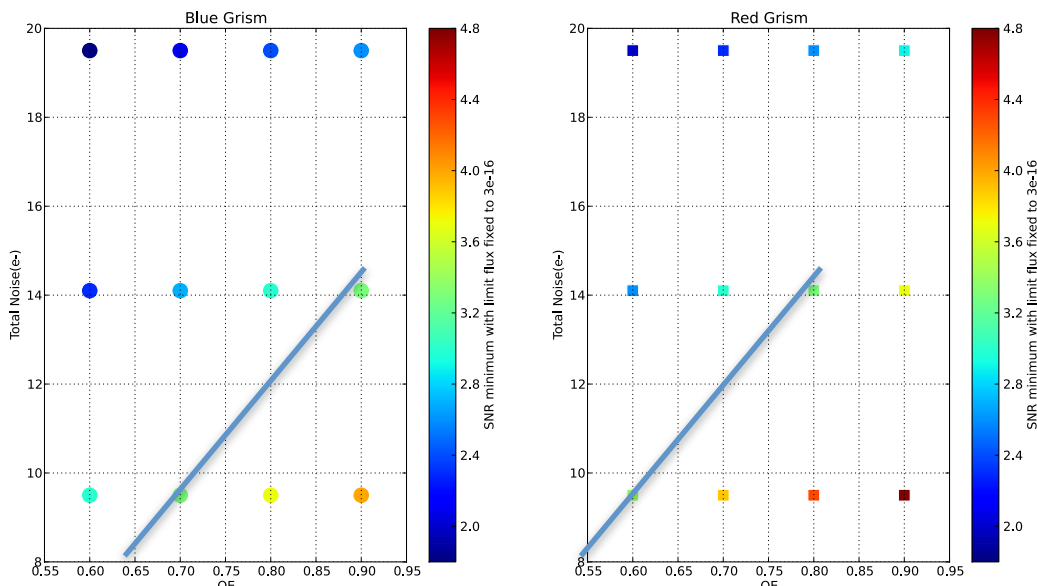


Figure 11: Total detector noise integrated on 560s versus the QE of the detector, all other parameters are fixed as described in Table 26. The green points correspond to the 3 sigma limit and the functional region for science is almost a linear extrapolation under the green points.

7.10.2.4. Estimation of the noise effect and validation of radiometric requirement

We have compared the prevision of the thermal analysis presented in RD6 with the budget introduced in the performance evaluation. The current worse estimation of 0,08 e/s/pixel for an warm telescope (included telescope and instrument) is well under the 20% of zodiacal noise as required in R-GC.2. For the stray-light, as already mentioned, it is too early to have a complete model and the first estimation of its variation inside the survey coverage, but has shown that this should be small if we can keep a low detector cut off .

7.10.2.5. Line flux limit versus wavelength

Figure 12 shows the flux limit in function of the wavelength, with the current instrument parameters as listed in Table 26, and 3 number of effective pixels: the line detection requirements GC.2.1.1 and GC.2.1.3 are satisfied even in the worst case and with 25 pixels under the line. It can be seen also than the strongest limitation is in the blue band on the lower wavelength (1.1 micron) where we have no margin at all. This was expected from the philosophy of the current configuration where all the values have been adjusted on the worst case configuration.

We have also evaluated on Figure 12, the degradation compared to the requirement, when we multiply the zodiacal value by a factor 2 or 3 as a worse case expecting in AD4. We see that in this case, we are marginal on the 2 wavelength edges (under 1,2 micron and upper 1,9 micron) with 25 pixels but we continue to be inside the requirement in most of the range.

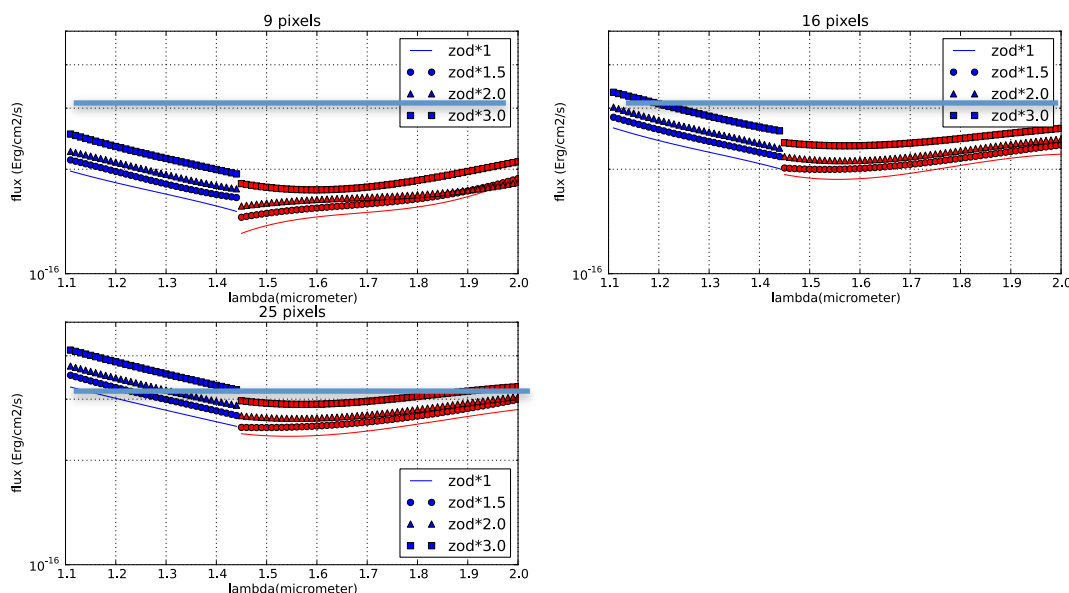


Figure 12: Flux limit with the standard zodiacal value and using a higher value (2 X and 3X) of zodiacal for 3 cases of number of pixel under the emission line. This is done with pixel size of 0,3”.

Let remain than there is a large possible performance gain expected if we can extract the line on less effective pixels, which is possible thanks to a better extraction code. We see than the effective gain can give a significant margin.

In Figure 13, we make the same exercise but with a pixel of 0,33”. Let remarks than, in principle, in this case, the number of pixel under the line should be smaller as the pixel coverage

is larger. Then there will be a compensation of the increase of zodiacal noise compared to the number of pixel in a realistic case.

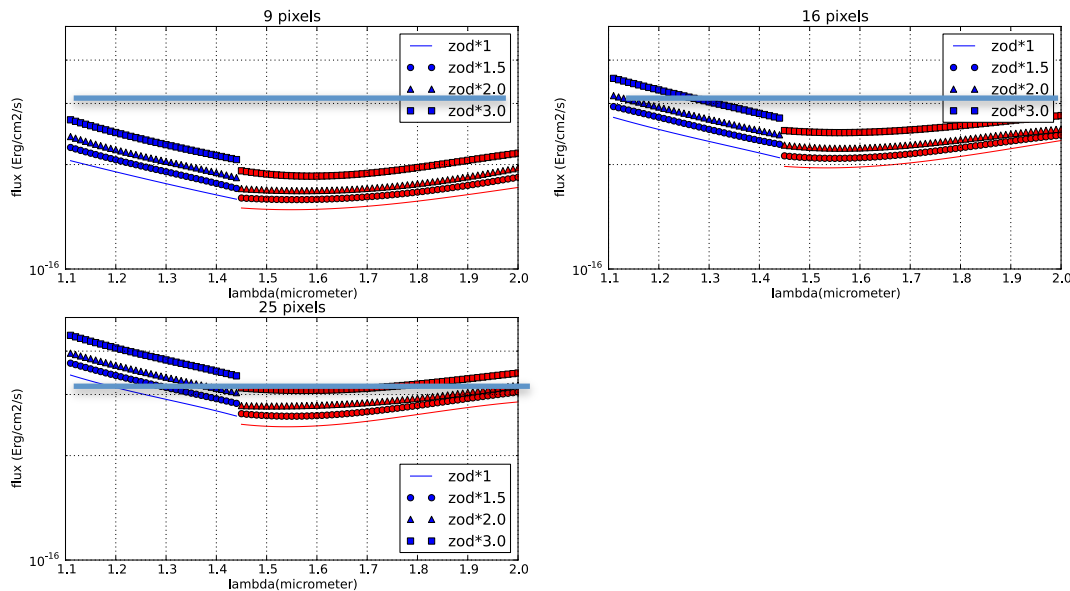


Figure 13: flux limit for a pixel size of 0,33" and different number of pixel under the line.

7.11. The completeness/purity performance validation

7.11.1. Method and Tools

7.11.1.1. Method description

Completeness is defined as the fraction of galaxies for which a redshift can be estimated, with a confidence greater or equal to a given threshold. This definition of completeness allows to select the best (and most pure, see below) sample.

For emission line galaxies, which are the primary targets for NISP slitless spectroscopy, the capability to measure a redshift depends on the capability to measure a line in the image for a given object. The first criterium is then on line strength which is directly linked to signal to noise and can be derived in instrument sensitivity as treated in the previous section.

In a slitless spectrograph, the second criterium to be estimated is the crowding in the field coming from other objects. Crowding not only can change the level of background around an object but will also contaminate spectra with “spurious” line coming from contaminating objects. At the depth of EUCLID spectroscopic observations, essentially every spectrum is at least partially superimposed to another, and contamination becomes the first reason for redshift measurement failures. The need for spectral contamination correction has lead to the choice of the observing strategy described above

Purity is defined as the fraction of objects contributing to completeness for which the redshift is correct within 3σ . In other words, purity gives the goodness of the selection obtained adopting a certain threshold for completeness. Purity of the sample is a level 1 requirement. While in simulations the purity is estimated by direct comparison with the known input value, during the mission it will be statistically estimated from a control sample derived from the Euclid deep survey.

Any attempt to fully scientifically evaluate the performances of the spectrograph, which implies measuring the completeness and the purity of the resulting sample, must therefore be capable of taking into account together instrument characteristics and observing strategy, and must implement within itself a spectrum extraction and redshift measurement method. For these reasons we have implemented a **full end to end simulation** chain is required. Such chain must not only take into considerations instrumental parameters and observing strategy, but also use an input catalog which is a fair representation of the universe, in terms of both spatial and redshift distribution of galaxies, and only at the end of this process, which is detailed below, we can safely demonstrate that we reach the degree of completeness and purity imposed by the requirements.

Only at the end of this process, which is detailed below, we can safely demonstrate that we reach the requested of the completeness in GC.2.1-2.

The implementation of this end to end simulation is shown on Figure 14 . It is based on different input catalogs to build an observational field (sky simulation) , an image simulation based on an instrument simulator, an extraction code of spectra (reduction pipeline) , and a code for redshift estimation and redshift reliability (redshift pipeline) . The complete chain has been developed and will be presented in this document.

To be able to disentangle between the effect of the instrument on the line extraction mainly coming from the image quality and the effect of the redshift measurement by itself, we have implemented and intermediate step, called later on '**toy simulation**', in which we can skip the redshift measurement to only estimate the signal-to-noise of line in the field in a statistical way on some realistic images. This can be done in a 'relative' way comparing the signal to noise of lines, when varying different instrument parameters that can affect the sensitivity or image quality of the field. This tool can be used to control and monitor any variation inside the image coming from the instrument. The two main parameters that can be monitor in this way are the PSF size in the field and the QE of the detector, from which the RMS can induce variation between pixel and detector. This tool and some results will be also presented in this document.

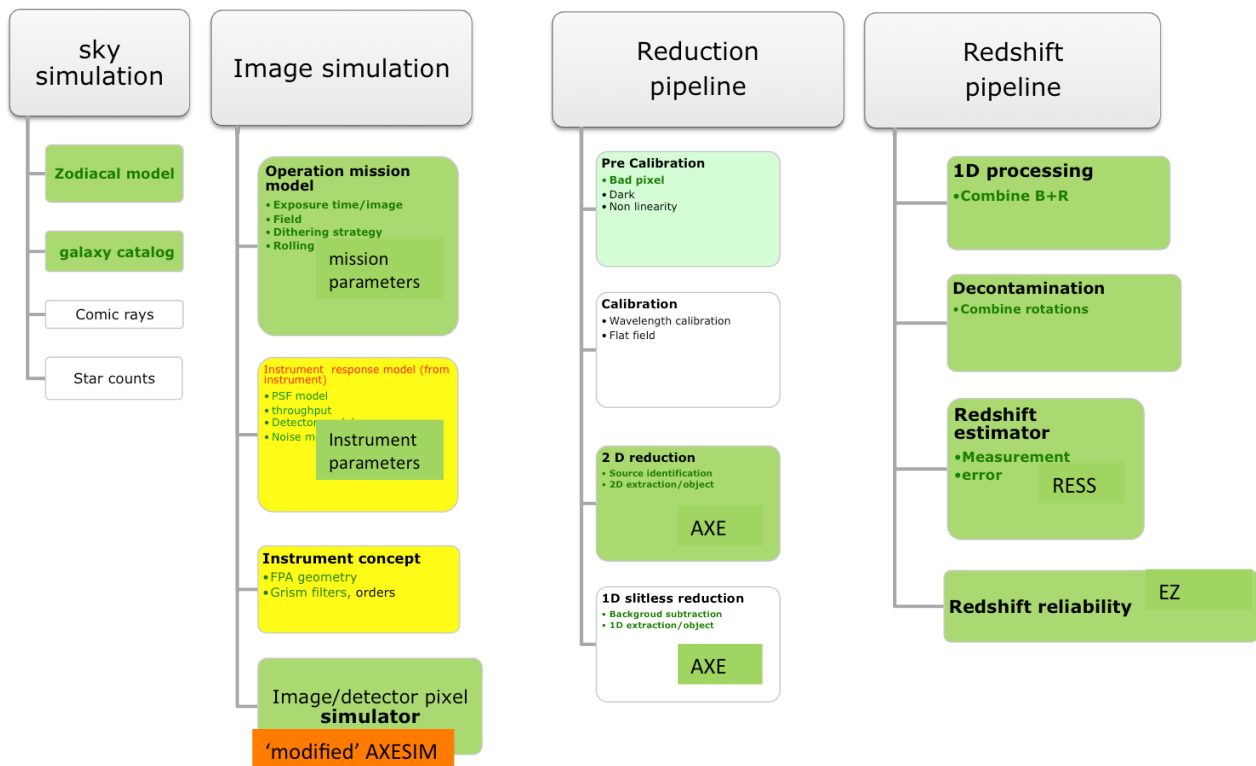


Figure 14: a scheme of the end to end pipeline needed to test completeness and purity. In yellow are indicated information's coming from the instrument, in green current implementation of codes, light green when it is partly done and in white boxes what will be added in further steps.

7.11.1.2. Construction of the observational field

Input Galaxy catalog:

The input is a representative catalog of objects with emission line H-alpha emitters with representative flux. Currently, we use the cosmos IRAC catalog (Ilbert et al. 2010, ApJ 709, 644) which covers >1sq.deg. For each galaxy it gives: sky coordinates, magnitude, stellar mass, Star Formation Rate (SFR), metallicity computed via SED fitting. SFR is converted into H α line flux, properly taking into account dust extinction, while metallicity is used to compute line ratios between H α and the other prominent spectra lines (O[II], O[III] doublet, H β). Each galaxy is then assigned a spectral type (early, intermediate, late) on the basis of the Specific Star

Formation Rate, and a matching spectral template, from the Bruzual and Charlot library. The H α galaxy counts of the catalog thus obtained are in fair agreement with published results (Geach et al. 2010, MNRAS 402,1330). Another fundamental ingredient for the realism of the simulation is the galaxy angular size. In slitless spectroscopy this is a crucial parameter, as it sets the effective spectral resolution and the level of confusion between adjacent spectra. An intrinsic and realistic angular size was thus assigned to each galaxy based either on the observed half-light radii re measured from the HST images of the COSMOS field, or on the size-luminosity relation when HST images were not available

In the end, for each object the catalog contains: sky coordinates, magnitude, galaxy size, H α line flux, flux for other lines, galaxy type.

Input Star catalog:

Currently two stars catalogs can be used, both derived from CFHTLS T0005 data: one for a high galactic latitude field, |b|=60 and another for a low galactic latitude, |b|=30, which gives about twice stars. Spectra for contaminating stars are created from the Pickles stellar templates, corresponding to the spectral and luminosity type, rescaled for each object to its magnitude. From |b|=60 to |b|=30 results do not change for more than 1 σ , and here we present only those obtained with the higher galactic latitude values.

Effects of even lower latitudes (and therefore higher stellar contamination), down to |b|=20 will be studied in the following months.

For each object, the catalog must contain: sky coordinates, magnitude, spectral type.

Zodiacal light:

The minimum value of zodiacal light has been adopted as level 0 value for all simulations (RD9). A different value for the zodiacal background will affect the results especially in the blue band, where it dominates the noise. By performing end to end simulations on smaller areas, we have derived some scaling relations as a function of the zodiacal light, which we apply to the main results to show its influence. More realistic results can be obtained by simulating a larger area (at least 1 sq degrees) with different values of zodiacal light, and combining results assigning to the results obtained with each zodiacal light value a weight which depends on how much of the survey will be conducted in those conditions. To do this a model for the survey strategy is needed and work is under progress.

Construction of the observed field

A contiguous area as large as the required survey area is located within the input catalog and subdivided into instrumental pointings; the list of objects falling inside each pointing is created. Each pointing is superimposed to a star catalog (derived from the CFHTLS T0005 data for W1 field, high galactic latitude, |b|=60 at a random position and all the stars falling into the pointing are added).

For each galaxy and star an incident spectrum is created. Galaxy spectra are created taking the continuum of the corresponding morphological type template and rescaling it to the object magnitude. The H α line with the correct flux and equivalent width as from the input catalog is

added upon the continuum and a standard set of lines is added ([OII], H β , [OIIIa], [OIIIb], [NII] and [SII]); fluxes for these lines are computed from the H α flux using standard lines ratios depending from the morphological type. Star spectra are created from the Pickles stellar template corresponding to the spectral and luminosity type, rescaled for each object to its magnitude. For each galaxy a 2D image is created using as structural parameters the values of r_{disk} , r_{bulge} and B/T stored in the catalog. 2D stars images are simulated using a Gaussian profile

7.11.1.3. The instrument simulator and the reduction pipeline

The actual spectra simulation, dither by dither, is completely carried out by the aXeSIM¹ code. Starting from the 2D undispersed images of each object in the field, aXeSIM creates a 2D direct image, and a 2D dispersed image. In the simulation, the following quantities are taken into account by means of a configuration file:

- Collecting area
- Global throughput
- System PSF
- Plate scale
- Detector parameters (RON, Dark current)
- Background noise
- Exposure time
- Wavelength coverage per grism
- Grism dispersion relation
- Total background

The total background is computed integrating the zodiacal signal within the observational wavelength range. The other parameters listed have the values indicated in Table 26

Figure 15 shows the output for a direct image simulation of the created field. Figure 16 is the counterpart dispersed simulated image in the blue band.

1 http://www.stecf.org/software/slitless_software/axesim/

The presented document is Proprietary information of the Euclid Consortium.
This document shall be used and disclosed by the receiving Party and its related entities (e.g. contractors and subcontractors) only for the purposes of fulfilling the receiving Party's responsibilities under the Euclid Project and that the identified and marked technical data shall not be disclosed or retransferred to any other entity without prior written permission of the document preparer.

Each dither is simulated separately, taking into account the observation strategy: the 2 grisms (blue and red) and 2 different roll angles. The dithering pattern is taken into account when simulating each dither: for each dither, the pointing is shifted by the appropriate dithering amount, and the spectra of galaxies near the FoV borders are truncated.

The simulations are carried out assuming that the coupling dither-observational strategy is as follows

Dither 1: Blue grism roll 0

Dither 2: Blue grism roll 90

Dither 3: red grism roll 0

Dither 4: red grism roll 90

The coupling between dither number on one side, and grism/roll configuration on the other side, has no impact on the results and this has been demonstrated by changing the coupling and comparing results.

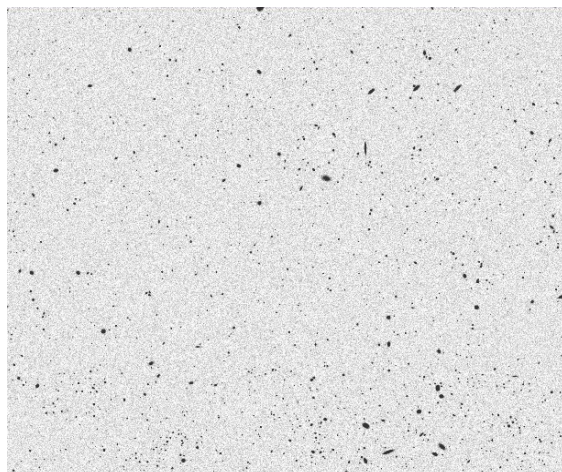


Figure 15: Example of a simulated direct image (single array)

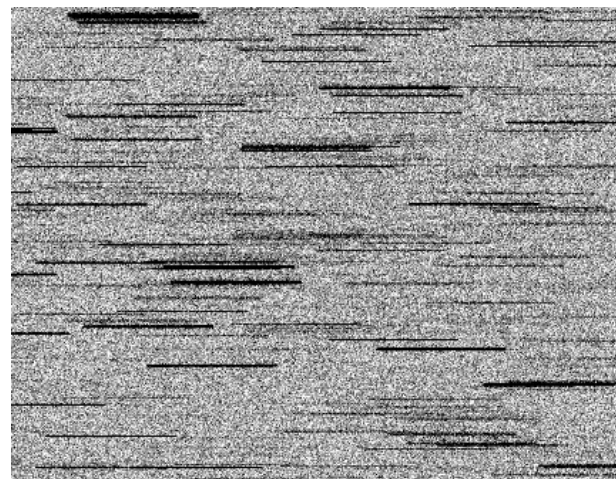


Figure 16: its dispersed counterpart in the blue band obtained with the aXeSIM software.

7.11.1.4. 1D spectra catalog production

The 2D dispersed image of each dither is then reduced by aXeSIM itself: spectra are extracted and calibrated in wavelength and flux. At this stage of the simulations, both wavelength and

flux calibration are assumed to be perfect. In particular, the sensitivity function used for flux calibration is directly derived from the total throughput curve. In the next implementations of the pipeline, wavelength and flux calibrations satisfying the requirements will be used.

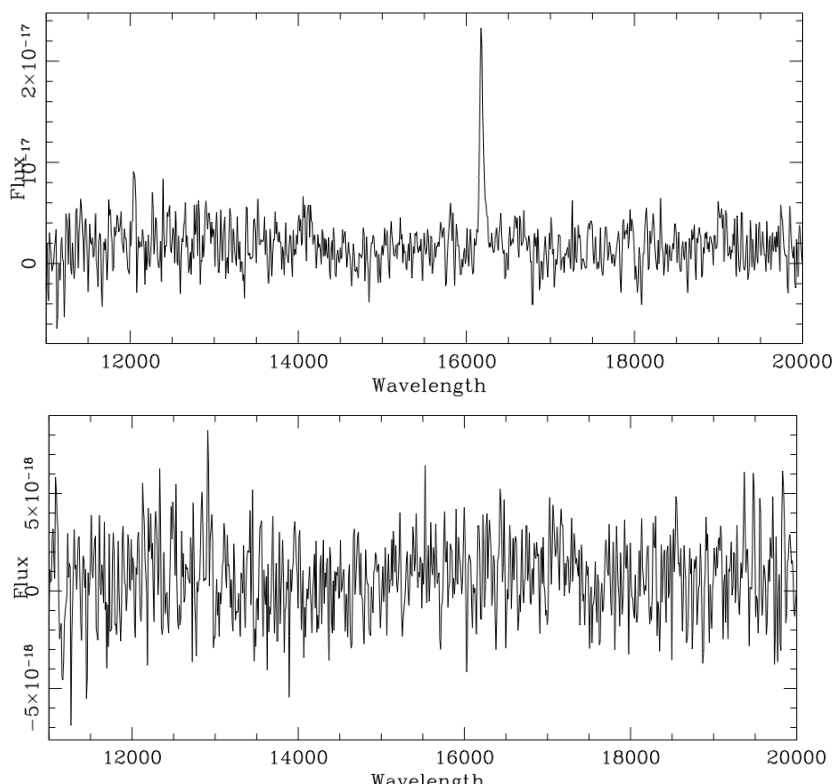
Once the 1D spectra for each dither have been produced, the spectra from the 2 bands for each roll angle are concatenated together (e.g. blue 0 and red 0, and blue 90 with red 90).

As the dithering pattern is part of the simulation process, the resulting spectra are already convolved by the FOV imprinting, i.e. they may present gaps in one (or both) of the two rolls, as shown in

7.11.1.5. Decontamination and redshift measurement (RESS)

Contamination is the first source of error when measuring redshift, and we use the advantage of having 2 different roll angles to check and flag spectra and features which can be contaminated. The procedure we currently adopt is the following

1. The 2 sub-spectra obtained with the 2 roll angles are subtracted one from the other: regions deviating from the zero level for more than the poissonian noise are considered contaminated and cut out from the corresponding input sub-spectrum. This allows to eliminate both contaminant emission lines and bright continua from contaminating objects (see **Figure 17** for an example). We thus obtain two decontaminated sub-spectra. More sophisticated algorithms for spectra decontamination are under study within the Ground Segment OU-SIR and OU-SPE groups, and will be used in the performance verification when available.



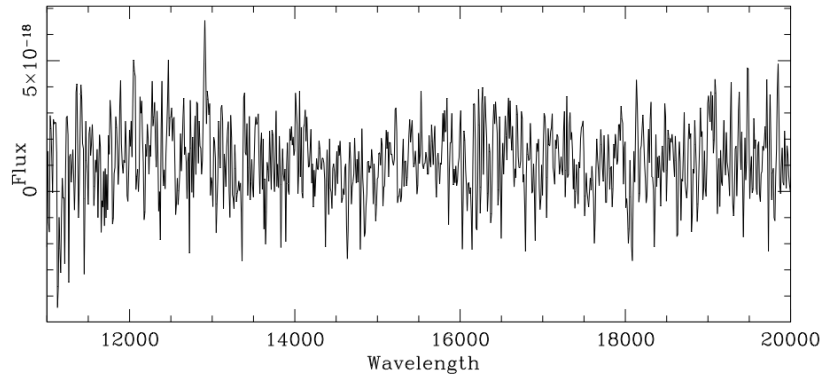
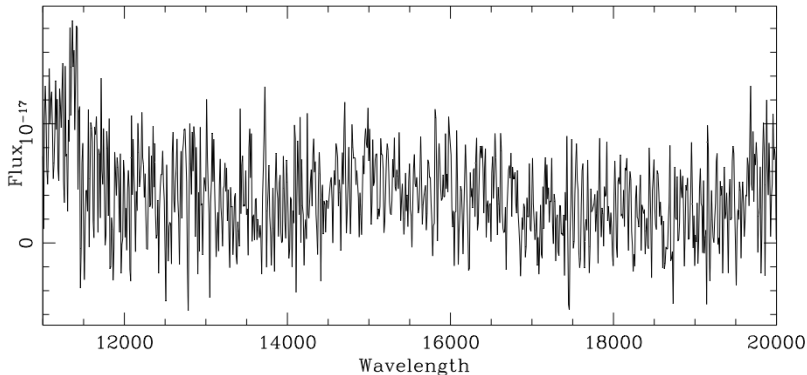
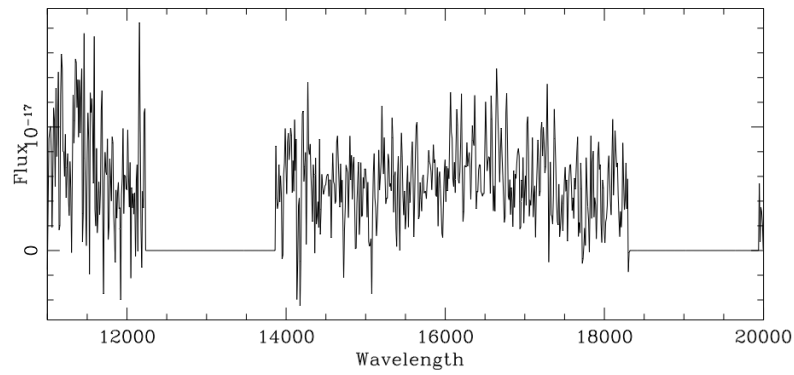


Figure 17: example of de-contamination. Top: roll 0 observation, the object line is visible at 1.3m, while a much stronger line is visible at 1.7 μ . Middle: roll 90 observation. The object line is (barely) visible at 1.3 μ . Bottom, the combined spectrum. Comparison from the 2 rolls has allowed to flag the strongest line as a contaminant



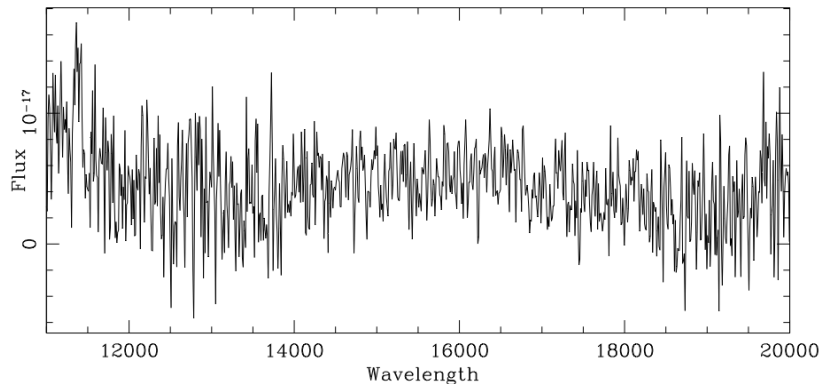


Figure 18: example of spectrum affect by gaps in the roll 0 configuration (top), but not in the roll 90 configuration (middle). The combined spectrum has a better S/N in the region observed in the two configurations

2. The two decontaminated sub-spectra are combined together, taking into account the possible presence of gaps (see Figure 18). In case of regions (or full spectra) with no signal (i.e. if both rolls are contaminated or if only one roll is available in that region because of the dithering pattern) the average operation is not performed and the combined spectrum is simply the sum of the two portions of spectra.

The **output** of this steps of the simulation is thus a set of “observed” spectra, clean from contamination.

At this point, redshift can be measured. In this process, we assume that photometric redshifts will be available allowing us to divide galaxies in three large groups: redshift range 0.7-2.0, where H α line is observable, the range $z > 2.0$ where the strongest emission line is [OII] (if present) or Ly α (at redshift > 4), and the low redshift regime where no strong emission lines are present. Such an *a priori* will be provided by the photometric redshift coming from Euclid photometry, with a given percentage of uncertainties. In the current simulations, we derive this knowledge from the input catalog, assuming (for the moment) a 0% of catastrophic misclassification. We exclude from analysis all objects lying outside the redshift range of interest for the requirement verification, ($z < 0.7$ and $z > 2.05$) and the following analysis is carried out only on this subset of objects. The redshift measurement is performed as follows

1. Look for possible emission lines.
2. Fit the continuum on the spectra using a spline of order 3
3. Measure the flux of emission lines referred to the local continuum level (measured in the neighborhood of each line): a Gaussian fit is performed and flux, EW and FWHM are measured from the Gaussian fit.
4. All emission lines are checked together to see whether they lead to a concordant redshift
5. When more than one emission line is detected but there is no "coincidence in z", the emission having the largest flux is assumed to be the "true" feature.

6. When only one feature is detected, it is assumed to be H α and the redshift is computed accordingly.
7. If no emission lines are detected the spectrum, a corr correlation technique is used (EZ, Garilli et al. 2010, PASP 122, 827)

Figure 19 and Figure 20 show two ‘one dimensional spectra’ extracted from the 2D image: the first is for a galaxy with a line flux of $\sim 4 \times 10^{-16}$, while the second shows a galaxy with an H α line flux of 8×10^{-16} . Also [OIII]a is visible in the observed range. Both spectra are obtained using the full 540sx4 dithers integration time.

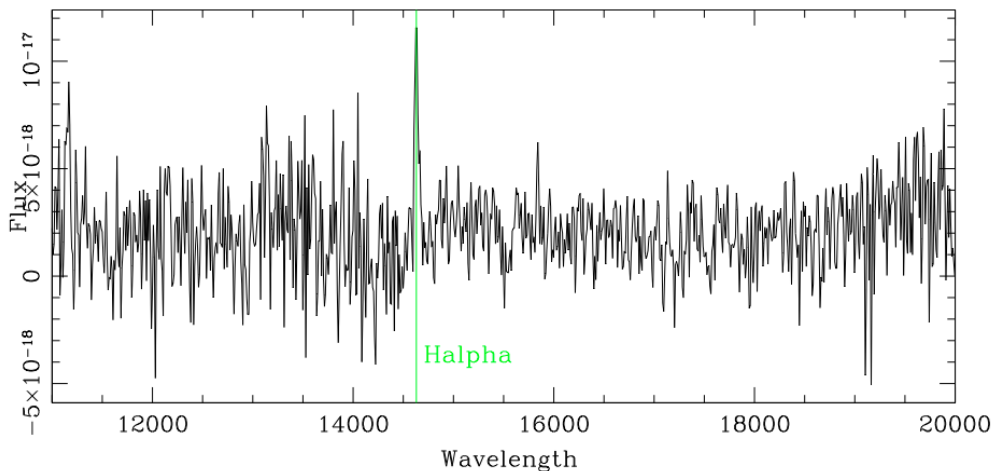


Figure 19; a simulated 1D spectrum with an H α emission line of 4×10^{-16} erg/cm 2 /s

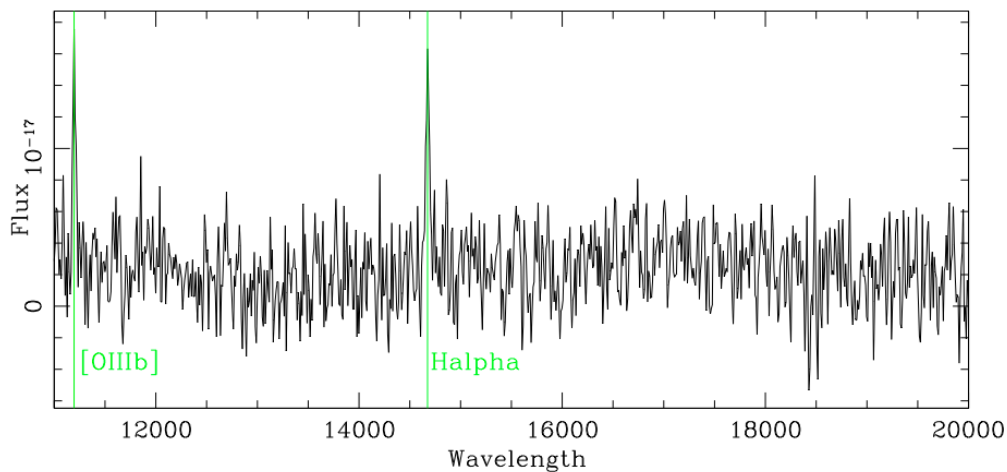


Figure 20: A 1D simulated spectrum with an H α emission line of 8×10^{-16} erg/cm 2 /s. the Oiii line is also visible in this example on the left edge.

7.11.1.6. Redshift reliability estimation

Finally, we use again EZ on the whole set of spectra to assign a reliability flag to each measure . The reliability concept is fully described in Garilli et al. 2010, PASP 122, 827, but it has been adapted to the Euclid case, where most spectra exhibit only one emission line. In few words: given the measured spectrum, we search on the combined final spectrum the expected emission lines (normally only H α , but in some cases also the oxygen doublet and H b). In this search, the detection threshold is set to a lower value than what used for the first detection above. If all, or most, the expected emission lines are detected, we assign a reliability of 90% or more. If only one line is found, but it has a high S/N, the reliability is set to 65%, while it lowers to 55% if the S/N is just above the detection threshold. Finally, if no line above detection threshold is found, we assign a reliability of 50%. The threshold above which a spectrum can be considered as reliable depends on the level of purity we want to attain. In this moment, we set a level of 65% or more.

The second output of the simulation is a catalog of objects with measured redshift and redshift reliability.

From this catalog, it is straightforward to estimate the completeness (i.e. the fraction of spectra measured above a given line flux limit) and the purity (i.e. the fraction of spectra for which the measured redshift is indeed correct).

The third output of the simulations are the tables of completeness and purity as a function of line flux, redshift, spatial coordinates.

This approach allows demonstrating attainability of level 1 requirements and of some level 2 requirements as the completeness.

7.11.2. Impact of the quality of the image on the completeness.

7.11.2.1. Rational and improved tool

Before presenting a full evaluation of the completeness for science, we present in this section some results with an intermediate tool developed to test the instrument quality in a ‘relative way’. The explanation of the full method is described in detail in RD9.

The current aXeSim code was difficult to modified to implement complex PSF or detector properties by pixel. Then we have developed a custom IRAF-independent Python wrapper that calls the aXeSIM core functions to generate 2D slitless images, and adds noise to them.

We also now have a throughout understanding of the C code, to eventually implement more advanced PSF or other variation easily. The code architecture is meant now to be highly modular compare to the standard aXeSIM code.. It is possible now to add on a slitless image a map of pixel which have different properties. In this way we can study any variation on a pixel to pixel basis or later on any variation in the field.

Our simulation code uses the CMC spectra and the EUCLID instrument parameters to generate images like the ones of the full pipeline, In this method anyway, the procedure to

generate one simulated image is separated in three steps. First we **simulate the sky**, then we multiply by the optical throughput and convolve by the PSF to **simulate the optical effects**. Finally we **simulate the detector noise** (in the following order: QE, dark-current, Poisson noise, Read noise). Each of these steps are independent and can be switched off. All the procedures are fully automatized in the Python wrapper. We just show the principle of the current code the Figure 21.

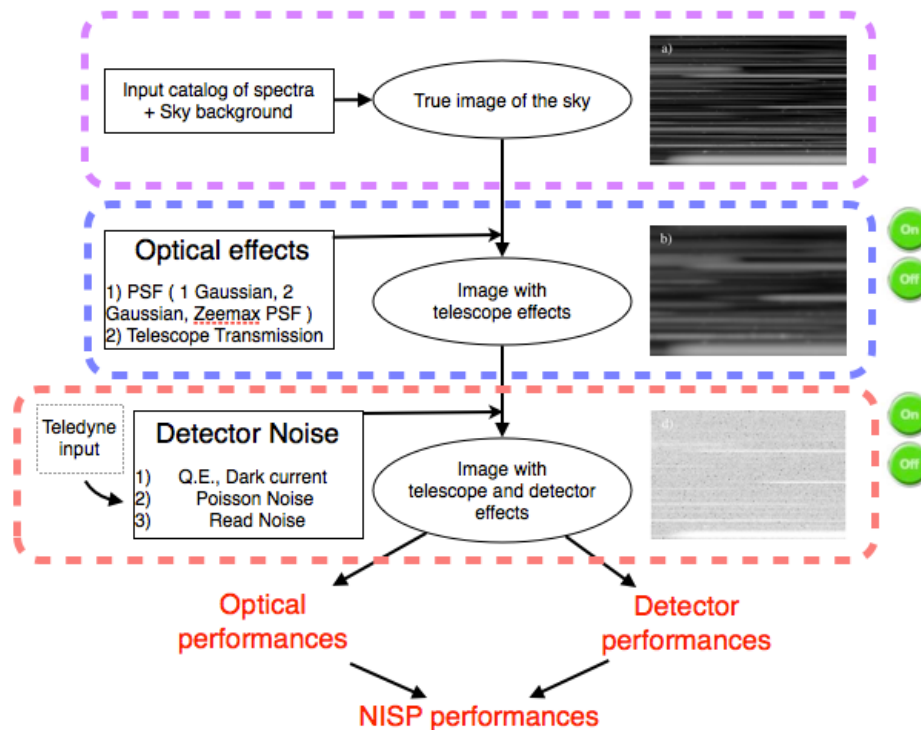


Figure 21: the modified aXeSim code for instrument evaluation

7.11.2.1.1. The test method

In this section, we describe how to evaluate the image quality only inside a simulated realistic field. We propose to study the PSF variation by filling the EE50-EE80 plan to measure relative completeness evaluation with PSF variation. We use the EE50-EE80 plan as it will correspond to instrument requirements and will be directly applicable. Here, we fix all other instrument parameters to their nominal values.

The method is to simulate the same image of the input catalog with different PSF and to do a full extraction and emission line estimation by a SNR evaluation. The final performance evaluation will be a comparison of the number of detected lines using only a signal-to-noise estimation with the different PSF.

As the generation of each image is a very heavy task (simulating an image with 30 000 spectra takes about 20 minutes) and to properly sample the plane EE50-EE80 at a minimal computing cost, we proceeded in the following way. It is possible to obtain a large number of double Gaussian PSF by summing together 2 Gaussian functions of width σ_i and σ_j , and a weight c varying between 0 and 1. This will allow also to test any PSF parameterized with a double Gaussian approach as the ones presented in section 7.4.2

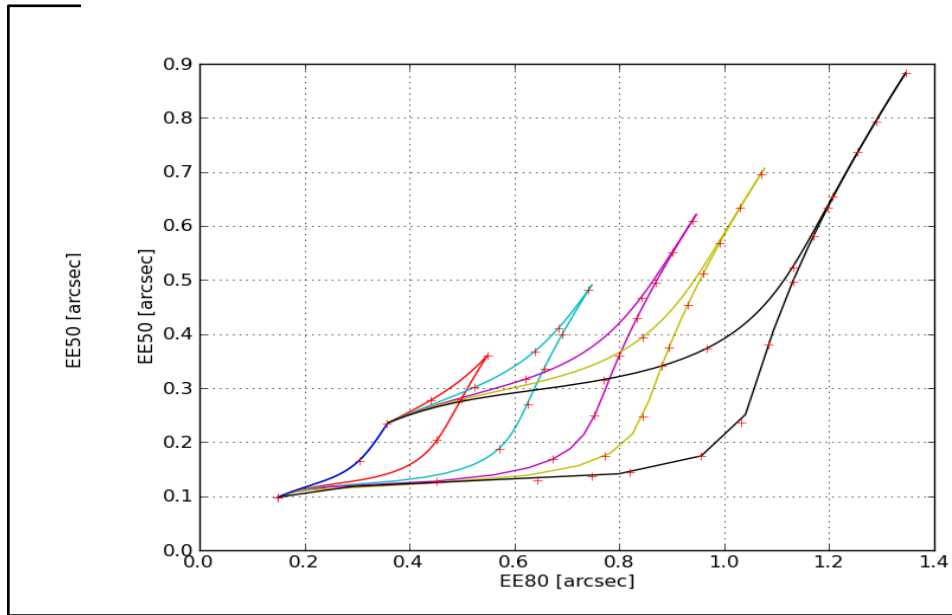


Figure 22: Sampling in the EE50–EE80 plane with 6 Gaussian functions with different width. Each colored curve is produced by varying the weight c from 0 to 1. The red crosses mark the pairs (EE50, EE80) that we probed in this analysis.

In this analysis, we simulated 6 times the same set of galaxies with 6 Gaussian PSF, and combined them with different weights c to produce 52 double Gaussian PSF. In **Figure 22**, the 52 red crosses correspond to the EE50–EE80 radius of the simulated double Gaussian PSF.

The analysis (estimation of number of line emission in the image) is focused to keep a relative performance evaluation of the instrument quality at instrument level, and to keep the analysis as close as possible of the sensitivity analysis. Our criteria will be based then on the object which have an Halpha emission line with $f_{H\alpha} > 3 \times 10^{-16}$ erg/cm²/s and to determine the variation of the SNR of this line due to image properties. To do so, we need two steps:

- A spectra extraction process : this is done by using the standard aXe code (Kümmel et al.2009).
- A line estimator based on SNR : The SNR is estimated from a Gaussian fit on the line flux.

We will compute the number of detected H α lines in one band with SNR >3 at a given flux limit.

We will apply exactly the same method for the detector variation. We will in this case, fixe the PSF and we will study the (QE, total noise) plan. To do so, we will add in each image a full

representative map of the pixel detector response including RMS and tails as provided by the vendor. We will only shift the mean value at the different values in the plan.

7.11.2.2. Results

7.11.2.2.1. PSF studies

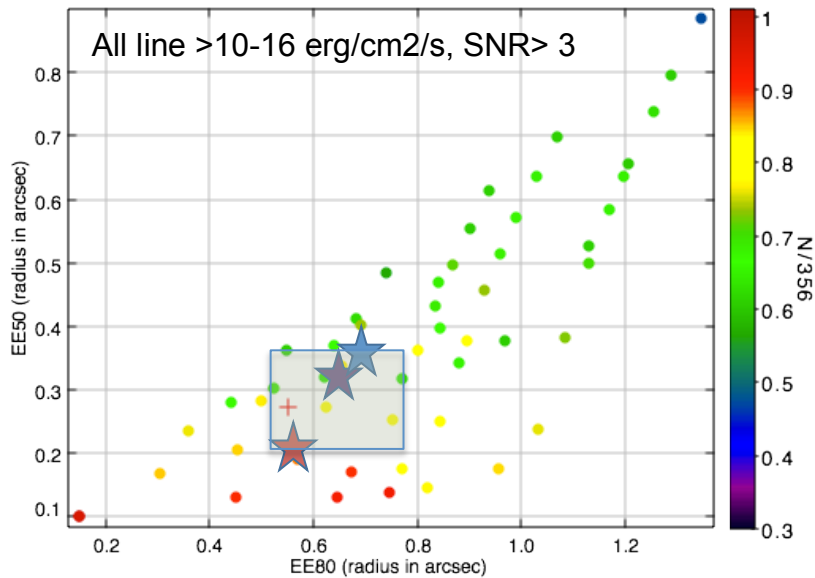


Figure 23: Percentage of $H\alpha$ emission lines with flux $f_{H\alpha} > 10^{-16}$ erg/cm²/s, observed with the R-grism setup and detected with SNR > 3. The cross indicate the current reference value used at IPRR. The different stars are the new values under evaluation (average, worst, worst+10%). The square indicate the expected level of variation of the PSF in the field.

We first plot on **Figure 23** all galaxies up the a flux $f_{H\alpha} > 1 \times 10^{-16}$ erg/cm²/s and SNR>3 in the red band (there is an identical plot for the blue band) to look at large variation in the field and see the impact of the PSF in all the EE50-EE80 plan. It is better to not cut at a flux limit on this plan, first to increase the statistic and avoid fluctuation, second to have possibility afterwards to change the flux limit and to study its impact.

To really do the PSF study, we now take the sample of galaxies with a flux $f_{H\alpha} > 3 \times 10^{-16}$ erg/cm²/s that correspond to the requirement for the flux limit, and count detected lines with SNR > 3 with the average PSF as reference sample: the ratio between this and the ones when we use the worst PSF and the worst + 10 % PSF as defined in **Table 21** gives us the relative lost due to the variation of the PSF in the field. We found a relative variation of less than 5 % as it can be seen in **Figure 24**.

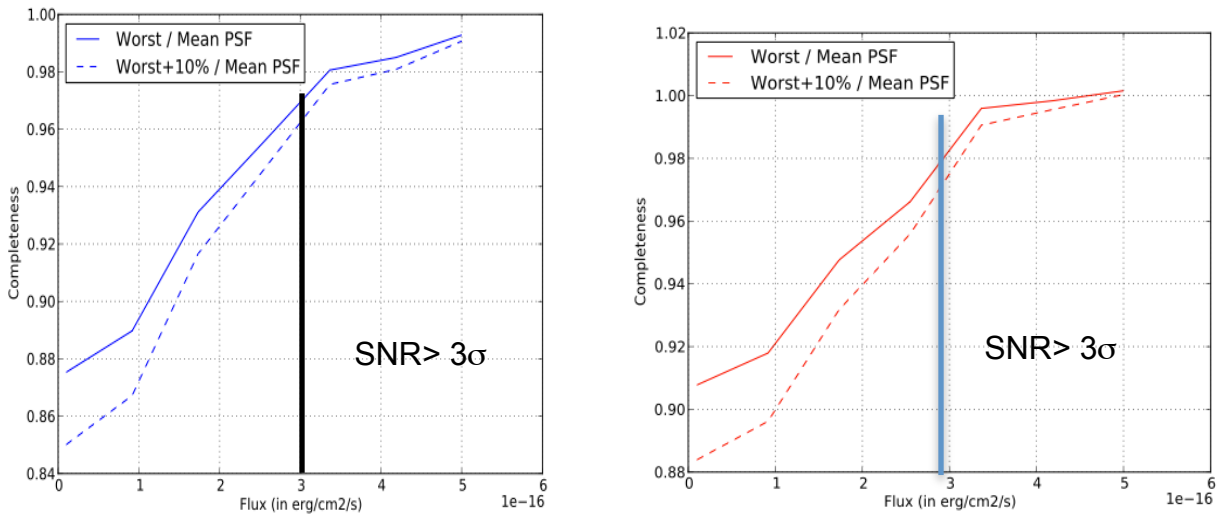


Figure 24: relative variation of the line with SNR> 3 from the average PSF to worst or worst + 10%. On the left for the blue band and on the right for the red band

7.11.2.2.2. Detector variation studies

We have done the same kind of studies to estimate the impact of detector properties on the

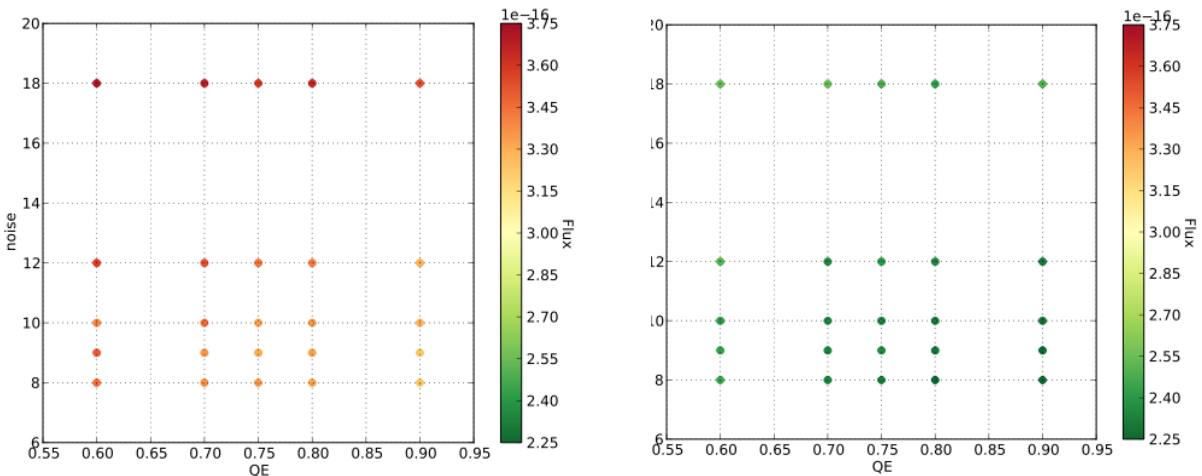


Figure 25: flux limit with the toy simulation of line reaching an SNR> 3 for the blue band (left) and the red band (right). The red band is more sensitive to line detection thanks to the lower zodiacal background

completeness..

We have simulated images with different mean values of QE and total noise but including a realistic RMS distribution of these parameters. We have then applied as a realistic detector processing (ie flat field) and made the same method of counting of galaxies above SNR>3 : the main conclusions are:

- the blue band is almost always near the limit flux of 3×10^{-16} erg/cm²/s whatever the detector is in the range $0.7 < \text{QE} < 0.9$ and noise $12 > N > 8$ (see Figure 25 left). The flux limit is well above the requirement in the red band: these results are well compatible with what we have seen with the ETC study.
- The fluctuation introduced by the RMS on these parameters is at the level of 5% in the 2 bands if we take only galaxies with a flux above 3×10^{-16} erg/cm²/s in the 2 bands and in the region of $\text{QE} > 70\%$ and total noise $< 10e$ (see).

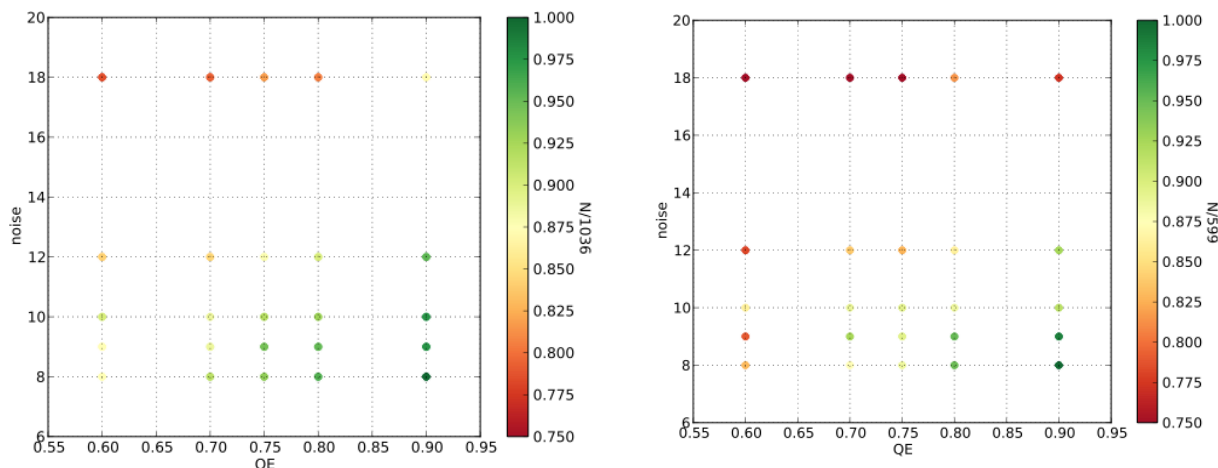


Figure 26; relative completeness on the blue band (left) and red band (right) when we vary the mean QE and noise RMS for all line $f > 1 \times 10^{-16}$ erg/cm²/s and SNR>3.

From this study, we conclude that the current specifications (AD5) for the detector will not introduce a significant degradation of the image quality for clustering and will be well inside the completeness budget. As expected, the observed degradation will affect mainly the line with a flux around 3×10^{-16} erg/s/cm² and are more sensitive in the blue part. For higher flux line, we observed almost no degradation in the 2 bands.

7.11.3. Completeness performance results with the full end to end pipeline

In this section we present the results obtained using the full scheme presented in **Figure 14** and described through 7.11.1.1. These results are based on a 1.3 sq. deg. simulation. In these simulations we have used the instrument parameters as from **Table 26**. We have evaluated also the influence of PSF on the results, and show results for the average case (WA) and the worst case (WW) case as described in 7.4.2 with the same double Gaussian approach. We have also performed

a first evaluation of the PSF degradation in the reddest part of the wavelength range, and these are labeled WR in the **Figure 27** (top panels) shows the completeness that is obtained in function of the true redshift (in differential form) and versus the emission H α line flux (in integral form).

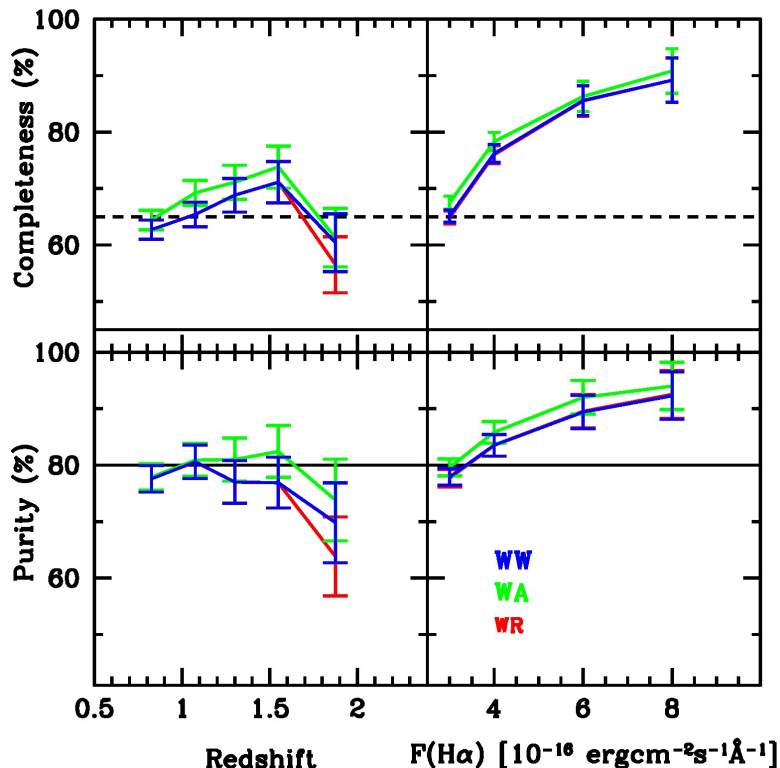


Figure 27 Completeness (top) and purity (bottom) evaluation using the current instrument and observational strategy implementation, for the three PSF cases WA, WW and WR (see text). The solid line indicates the current requirement, log-dashed line is the current goal. Error bars indicate purely poissonian fluctuations.

The requirement of completeness GC.2.2-2 above 45% is fully met on all the range with significant margins. We see that the global impact of the PSF degradation is more sensitive in the reddest part but stay within 5% of degradation in all the range. This is in very good agreement with the toy simulation (see Figure 24).

7.11.4. Inoperability of pixels

In the case of spectroscopy, the science requirement is based on a line detection which is spread in average for an object size of 0,3'' (mean size of the objects expected in the survey) on 3x3 pixels. This means than any dead pixel will degrade the detection but we expect to not loose strong lines as we can extrapolate it on the others pixels. Then we assume than only the objects which have a flux < 5 10 $^{-16}$ erg/cm 2 /s will be affected. These are the first two bins of **Figure 27** top right.

The presented document is Proprietary information of the Euclid Consortium.

This document shall be used and disclosed by the receiving Party and its related entities (e.g. contractors and subcontractors) only for the purposes of fulfilling the receiving Party's responsibilities under the Euclid Project and that the identified and marked technical data shall not be disclosed or retransferred to any other entity without prior written permission of the document preparer.

A first evaluation gives than with 5% of dead pixel, there is 20 % of probability to have a dead pixel under a line but only 6 % of them have a flux $< 5 \cdot 10^{-16}$ erg/cm²/s. Looking at **Figure 27**, we see that we still have such a margin on the completeness requirement.

Then in conclusion this should have an impact on sensitivity only for low flux lines and we estimate that we can accept a 10% rate of inoperable pixels EOL. This has been be verified with toy simulation where tails can be introduced to mimic dead or bad pixels. The current detector maps are very good with less than 2 % of non operable pixels which have very little impact on the result and is under the specification of 5%.

To better study this effect, we will simulate larger tails in further simulation to test exactly the limit we can accept on non operable pixels.

7.12. Spectroscopy level 1 requirements to NISP performance

7.12.1. Level 1 requirements

In this document we address the verification of some level 1 requirements that have been tested using the end to end simulation described in section 7.11 and are listed in Table 27. The rational and more detail on the impact of these results on clustering performance can be found also in the mission performance document (RD10).

	Description	Requirement	WA	WR
GC.1-2	Galaxy sky density	$3,500 / \text{deg}^2$	YES	YES
GC.1-3	Redshift accuracy	$\sigma(z) < 0.001(1+z)$	YES	YES
GC.1-4	Systematic offset in redshift	<1/5 redshift accuracy	YES	YES
GC.1-6	Median of redshift distribution	>1	YES	YES
GC.1-7	Upper quartile of redshifts	>1.35	YES	YES
GC.1-10	fraction of catastrophic failures	$f < 20\%$	YES	Within 1σ
GC.1-11	fraction of catastrophic failures	known to 1%	YES*	
GC.1-12	mean redshift in 0.1 redshift bin	known to 0.1%	Within 1σ *	
GC.2.1-10	Subsample of galaxies	$>140,000$ gals, with $>99\%$ purity	YES*	

Table 27: Spectroscopic Level 1 requirement validation. Items marked with * are verified through deep survey simulations

7.12.2. Results

7.12.2.1. Purity (R-GC.1.11)

Using the output of simulations we can evaluate what is the fraction of redshift, which are considered good and reliable by the extraction, but in effect are wrong, as the truth is known from the simulation: this ratio is called purity which is the exact complement the fraction of catastrophic redshifts as defined in R-GC.1-10. **Figure 27** (bottom panels) shows the purity of the sample as from the latest evaluation. The 80% purity requirement is met within 1σ in the WA simulations. In the last redshift bin, purity shows a decrease, so that both WW and WR are not compliant with the requirement.

There are several factors contributing to such a decrease:

1. At $z > 1.8$, [OII] comes in the visible range, and can be mismatched for H α
2. H α falls in a region where throughput is 10% less than the region where [OIII]_a or H b fall. If these lines are of comparable emitted intensity (high metallicity objects), [OIII]_a has a higher S/N than H α and we have a line mismatching
3. For the same reason as above, at the flux limit H α is not detected, while [OIII]_a is
4. The chance of contamination is higher at spectrum edges than in the center, which again can diminish the S/N of H α line

The fulfillment of this requirement depends very much on data processing, and further improvements will be possible and made using for example photo-z information to break any line degeneracy.

7.12.2.2. Redshift accuracy (R-GC.1.3 and R-GC.1.4)

By comparing measured redshifts with input true values, we can compute the mean difference between measured and true redshift. Figure 28 left, shows the difference between measured and true redshift as a function of the true redshifts. The thin black lines indicate $\sigma(z) < 0.001(1+z)$, as requested from R-GC.1-3. 92% of the galaxies are within 3 sigma of the required limit. Figure 28, right shows the distribution of the difference between the measured and true redshift. In the 2 plots, only objects contributing to completeness are shown (i.e. the two figures include 20% of catastrophic redshift)

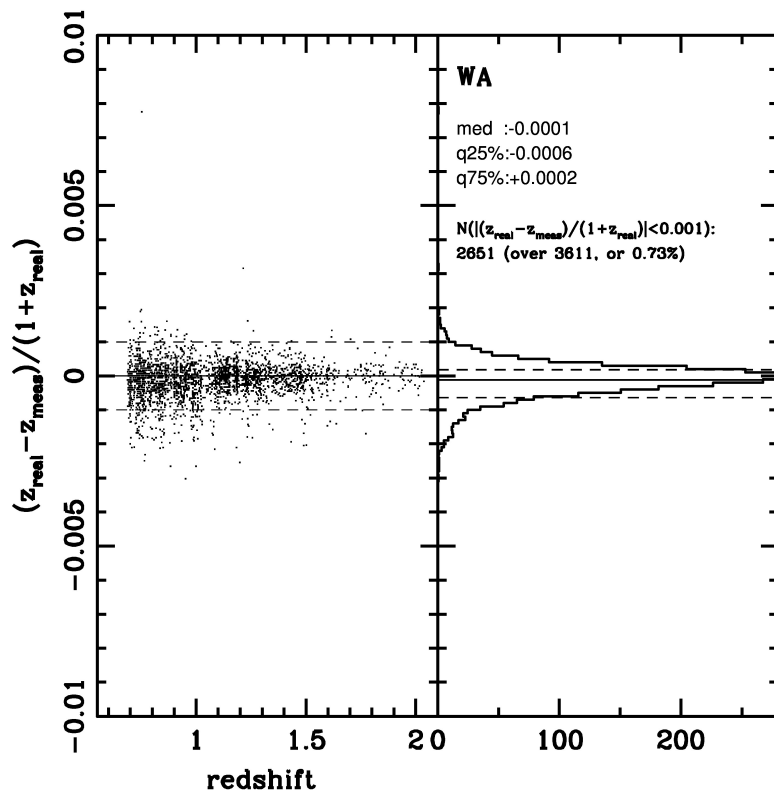


Figure 28: Left: difference between true and measured redshift as a function of the true one. The figures include all objects contributing to completeness. The dashed lines show the required 1sigma distribution. Right: Difference between the measured and true redshift

The mean absolute difference for the good measurements is $1 \cdot 10^{-4}$, perfectly satisfying R-GC.1-4, which requires a systematic offset $< 2 \cdot 10^{-4}$

The redshift accuracy requirement is satisfied within 1s (73% of the objects lie within the requested accuracy limits), as also shown by the distribution quartiles

7.12.2.3. Verification of the redshift distribution and galaxy density requirements

From the simulation results using the second output catalog with objects, redshift and reliability, we can build the galaxy density (dn/dz) distribution which is the number of galaxies with a good redshift in function of redshift. The distribution is represented on **Figure 29** (See the mission performance document (RD10) for more detail of the use of this distribution on clustering). This distribution is anyway fully representative of the one we expect to reconstruct to do the science clustering. The impact of the SPF variation on the full distribution is shown and is inside the current error bar of 5%.

The median of this dn/dz distribution is currently $z=1.4$ (R-GC.1.6 asks to median $z > 1$) and the

upper quartile of the redshift distribution of galaxies with redshift > 0.7 is $z=1.7$ (requirement R-GC.1.7 is upper quadrille >1.35)

Finally, we can also verify the expected sky density of measured objects with redshifts to match R-GC.1-2 of $> 3,500$ galaxies/deg²

After normalisation, we end up with 4300 galaxies per sq. deg which is well in agreement with R-GC.1.2 to have more than 3500 galaxies/ sq. deg

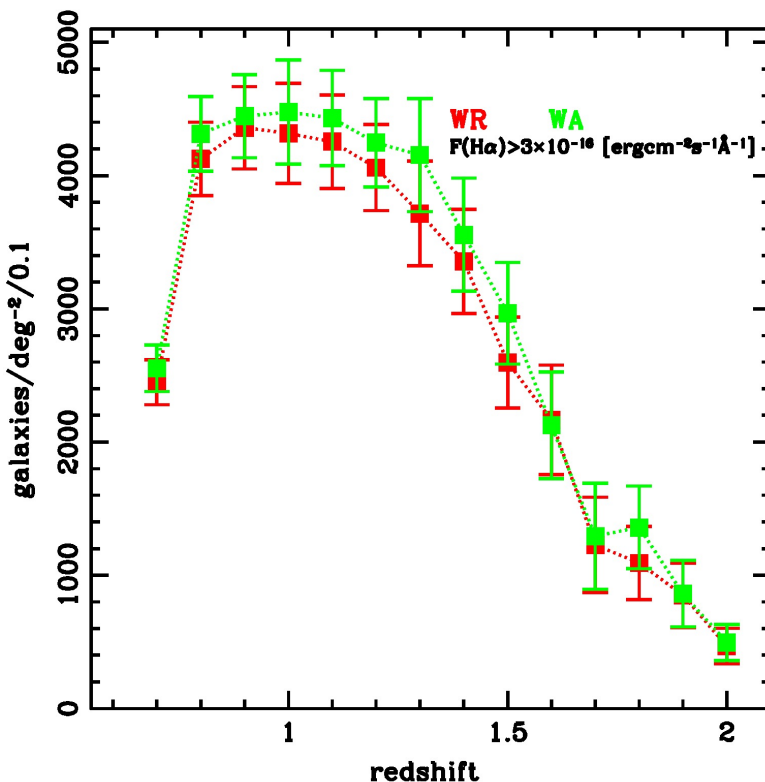


Figure 29: The galaxy density distribution reconstructed with the end-to-end simulation with the current implementation for 2 PSF (average WA and reddest one WR). This distribution fulfills all requested Level 1 requirements.

7.12.1. Deep survey simulation

The deep survey has a fundamental importance, as it shall provide a pure at 99% sample of at least 140 000 galaxies (GC2.2-10), which shall be used to study the systematics of the wide survey (requirements GC.1-11, GC.1-12, and GC.2.1-10) and correct the effect of the selection (mainly the 20% of catastrophic redshift).

The concept underlying these requirements are that by performing several wide-like observations (i.e. 2rolls + 2 grisms), contamination may be better be accounted for and can be corrected.

We have simulated a small area using the same area as the wide survey, “rotating” the field by 15 degrees at each wide-like observation (4 dithers each), to check how many of such observations are required to reach the requested completeness, purity and galaxy density. Results are shown in

Figure 30. From the left panel, it can be seen that the 99% completeness requirement is fully reachable performing 12 wide-like observations (for a total of 24 rolls), and reached within 1σ with 9 wide-like observations. Analogously, purity requires at least 9 wide-like observations. The statistics of these simulations is rather low, due to the long computational time required, so that it is not clear whether the difference in completeness and purity is significant. A larger area will be simulated in the near future to distinguish between these two cases.

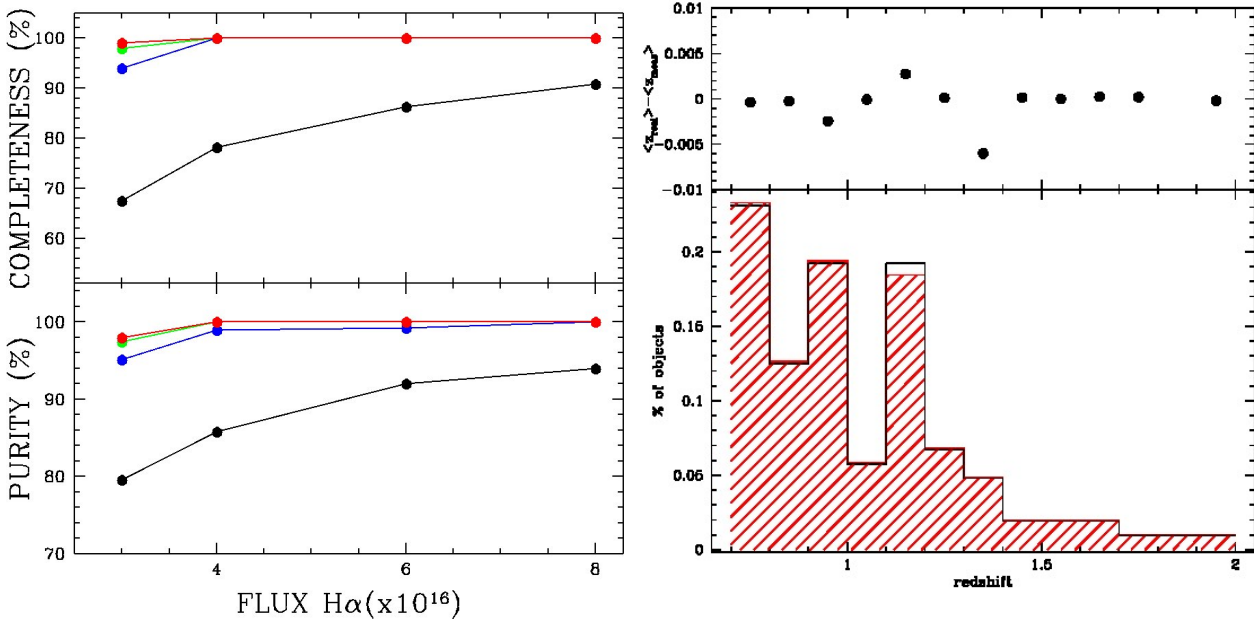


Figure 30: deep survey simulations. Left: completeness and purity reached with 1 wide observation (black line), 6 wide-like observations (blue), 9 wide-like observations (green) and 12 wide-like observations (red). **Right:** real (black empty) and observed (red dashed) redshift distribution from the Deep survey. The top panel shows the difference between the mean redshift of the true distribution and the observed distribution

The right panel of **Figure 30** shows the fulfillment of GC.1-12 in the case of a deep survey performed with at least 12 wide-like observations. The threshold of deviations smaller than 0.1% is fully reached almost in every bin. Given the small statistics involved, deviations from the requirement cannot be considered significant, and more simulations are needed to fully confirm this requirement.

Finally, given the completeness and purity obtained, and assuming an underlying population as from Geach et al. 2010, the galaxy density we reach is above 19000 gal/sq. Deg., well above the required number if we consider a deep field of 40 deg².

7.12.2. About zodiacal light

All results presented so far have been obtained using the minimal value of zodiacal light. As the survey will cover few thousands of square degrees, the zodiacal light will vary from sky region to sky region, thus the background can be higher and as a consequence performances lower.

In Table 28, we show the dependence of galaxy density, completeness and purity as a function of zodiacal light.

	Minimal zodi light			2*zodiacal light			3*zodiacal light		
	Gal/deg	compl	purity	Gal/deg	compl	purity	Gal/deg	compl	purity
WA	4037	~68%	~80%	3445	~60%	~72%	2995	~57%	~63%
WR	3762	~65%	~78%	3221	~60%	~71%	2809	~54%	~62%

Table 28: galaxy density, completeness and purity as a function of zodiacal light

When the zodiacal light is doubled, in both WA and WR cases we are still compliant in completeness and galaxy density (within 1s). The purity value looks low, but it is also still within 1s. When the zodiacal light becomes 3 times the minimum value, the requirements cannot be fulfilled. We can apply the above scaling relations to the redshift distribution as shown in Figure 31.

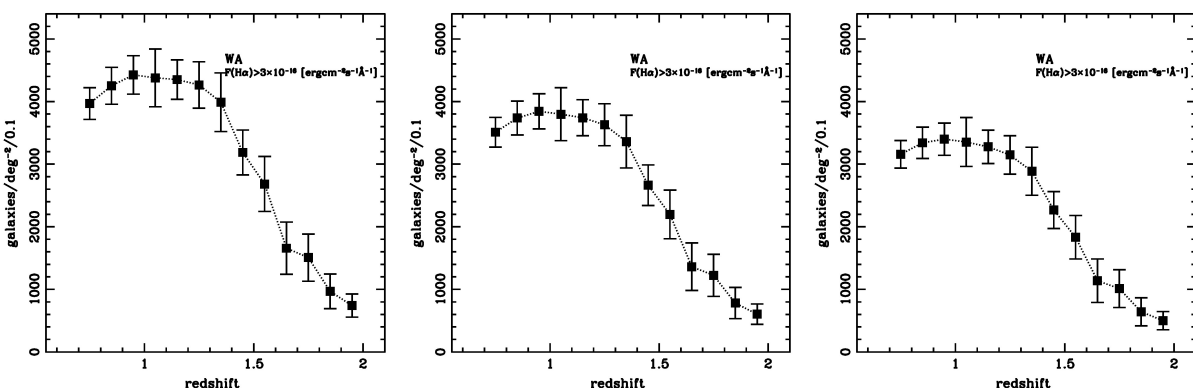


Figure 31: redshift distribution obtained with a minimum zodiacal light as from requirement (left), with 2* minimal value (center) and with 3*minimal value (right)

A more precise evaluation of the influence of zodiacal light on the whole survey will be possible by convolving these results with some possible observing strategies

7.13. Future plan

The end-to-end simulation will be discussed and merged with new codes developed for simulation and data reduction in the SGS framework. Although the current version of the end-to-end simulations is already at an acceptable level of sophistication, there are still a number of improvements to be made to fully take into account all instrument and data reduction characteristics that will be reviewed in the next phases.